ABSTRACT

Title	A Lattice Kinetic Scheme with Grid Refinement for 3D Resistive Magnetohydrodynamics
Candidate	Bryan R. Osborn
Degree and Year	Master of Science, 2004
Thesis Committee	William D. Dorland, Chair Assistant Professor of Physics
	Adil B. Hassam Professor of Physics
	C. David Levermore Professor of Mathematics

We develop, analyze, and numerically test a 3D lattice kinetic scheme for the resistive magnetohydrodynamic (MHD) equations. This scheme is based on the square D3Q19 lattice for the fluid and the square D3Q7 lattice for the magnetic field. The scheme is shown to be consistent with the MHD equations in the low-Mach, high-β limit. We numerically test the scheme in a pseudo-3D implementation by examining its reproduction of linear MHD eigenmodes as well as its performance on the non-linear Orszag-Tang problem. Results show that the waves are correctly reproduced and that the code has second-order convergence in time step and grid spacing. A multi-block refinement algorithm is then tested, and its convergence properties are examined for the non-linear Orszag-Tang problem. We conclude that this multi-block refinement algorithm—previously only applied to hydrodynamic lattice kinetic schemes—can be used in conjunction with MHD lattice kinetic schemes.

A Lattice Kinetic Scheme with Grid Refinement for 3D Resistive Magnetohydrodynamics

by

Bryan R. Osborn

Thesis Submitted to the Faculty of the Graduate School of the University of Maryland, College Park in Partial Fullfillment of the Requirements for the Degree of

Master of Science
2004

Advisory Committee:

William D. Dorland, Chair
Assistant Professor of Physics

Adil B. Hassam
Professor of Physics

C. David Levermore
Professor of Mathematics

Table of Contents

List of Figures

Chapter 1
Introduction

In this thesis we present the development of a lattice kinetic scheme for solving the standard set of resistive MHD equations

$$\partial_t \rho + \nabla \cdot (\rho \mathbf{u}) = 0 \tag{1.1}$$

$$\partial_t (\rho \mathbf{u}) + \nabla \cdot (\rho \mathbf{u}\mathbf{u}) + \nabla p - (\nabla \times \mathbf{B}) \times \mathbf{B} = \nabla \cdot (2\nu\rho\mathbf{S}) \tag{1.2}$$

$$\partial_t \mathbf{B} + \nabla \times (\eta \nabla \times \mathbf{B} - \mathbf{u} \times \mathbf{B}) = 0 \tag{1.3}$$

with isothermal closure

$$p = \left[\frac{k_B T}{m}\right] \rho \tag{1.4}$$

and strain tensor

$$\mathbf{S} = \frac{1}{2}\left[\nabla \mathbf{u} + (\nabla \mathbf{u})^{\mathrm{T}}\right].* \tag{1.5}$$

These coupled partial differential equations describe the evolution of plasmas as diverse as liquid metals, fusion plasmas, and astro-physical plasmas [23]. The canonical set of numerical methods used for the solution of these equations includes pseudo-spectral methods, finite-difference methods, and finite element methods. Each of these standard methods solves the resistive MHD equations through direct discretization of the field Eqs.(1.1), (1.2), and (1.3). The main challenge in such discretizations is the evaluation of the nonlinear flux derivatives—one of which is the $\nabla \cdot (\rho\mathbf{u}\mathbf{u})$ term in Eq.(1.2)—in such a way that mass, momentum, and energy are properly conserved [27]. In high-dimensional systems with many field variables, such methods can quickly become tedious to implement and analyze.

*This strain tensor gives rise to the standard shear viscosity $\nu\rho\nabla^2\mathbf{u}$ as well as a bulk viscosity. For an extensive discussion of these viscosities in relation to lattice Boltzmann methods, see [10]. We adopt this form because it is the form that will arise from the Chapman-Enskog expansion of our scheme.

Lattice Boltzmann methods (LBMs) provide an alternative for solving PDE systems that arise from a kinetic theory. The LBMs rely on the linear nature of the convective derivative in the Boltzmann equation

$$\partial_t f + \mathbf{v} \cdot \nabla f + \frac{\mathbf{F}}{m} \cdot \nabla_{\mathbf{v}} f = \left(\frac{df}{dt} \right)_c \tag{1.6}$$

to build elegant and simple-to-implement numerical schemes which recover the macroscopic field variables ρ and $\rho\mathbf{u}$ by taking moments of f (as discussed in the next section). The resulting methods are also amenable to parallelization as they are fully explicit and local. Perhaps the strongest argument in favor of further investigation of the LBM is its ability to address multi-phase flows, multi-component flows, flows through porous media, and flows near complex boundaries: these are areas where traditional methods can fall somewhat short [5][6].

The second major component of this thesis is the application of the grid-refinement scheme in [12][11] to pseudo-3D MHD. The refinement scheme derived and discussed in these references allows block-refinement of the spatial domain. By selectively refining the spatial grid near small-scale structures, we can avoid the computational overhead of needlessly refining the entire domain. In [21], the authors use a 2D LBM with multi-block grid refinement to simulate flows near an airfoil. In MHD, such local flow structures can occur in, for example, tearing mode reconnection [14] which is relevant to many astrophysical problems. In this type of reconnection, a thin current layer forms near the reconnection point. This layer is important to resolve because it drives the reconnection rate. To resolve this layer without a grid refinement scheme one is forced to use a finely discretized grid over the entire domain. Refining the grid near this current layer would allow much lower resistivities to be obtained by focusing computational effort on the thin current sheet. More generally, any problem involving shocks—such as a coronal mass ejection—would benefit from an adapative refinement scheme based on block-refinement.

To date, the only application of grid refinement to LBM MHD has been restricted

to 1D [16]. Here we will apply the multi-block refinement method described in [12] to our lattice kinetic MHD method in a pseudo-3D case and verify numerically that the resulting method can properly recover the MHD equations across inter-block boundaries in linear and non-linear problems.

Chapter 2
The Lattice Boltzmann Method

2.1 The Boltzmann Equation

Lattice Boltzmann methods are numerical methods for solving systems of PDEs that arise from an underlying kinetic theory. Before we delve into the derivation of an LBM for the MHD equations, it is appropriate to examine a simpler system, the Navier-Stokes equations:

$$\partial_t \rho + \nabla \cdot (\rho \mathbf{u}) = 0 \tag{2.1}$$

$$\partial_t (\rho \mathbf{u}) + \nabla \cdot (\rho \mathbf{u}\mathbf{u}) + \nabla p = \nabla \cdot (2\nu\rho \mathbf{S}). \tag{2.2}$$

We again assume an isothermal closure. This system describes the evolution of a compressible fluid with mass density $\rho(\mathbf{x}, t)$ and flow velocity $\mathbf{u}(\mathbf{x}, t)$. To arrive at these equations, one can use the classical, purely phenomenological reasoning as in [28]. A second approach is to derive these equations from first principles. This second approach—forming one branch of kinetic theory—suggests an alternative to the popular numerical methods used to solve Eq.(2.1) and Eq.(2.2).

Instead of directly discretizing Eq.(2.1) and (2.2) as in the standard numerical methods, the LBM considers the more fundamental Boltzmann equation

$$\partial_t f + \mathbf{v} \cdot \nabla f + \frac{\mathbf{F}}{m} \cdot \nabla_{\mathbf{v}} f = \left(\frac{df}{dt} \right)_c . \tag{2.3}$$

This equation describes the evolution of $f(\mathbf{x}, \mathbf{v}, t)$, the number density of particles at position $\mathbf{x}$ moving with velocity $\mathbf{v}$. The RHS accounts for the effects of particle collisions while the third term on the LHS is called the body-force term and accounts for any external forces acting on the particles. The LBM solves Eqs.(2.1) and (2.2) by discretizing

(2.3) and recovering the macroscopic fluid variables ρ and $\rho\mathbf{u}$* by taking the appropriate moments of f:

$$\rho(\mathbf{x},t) = m\int f(\mathbf{x},\mathbf{v},t)d\mathbf{v} \tag{2.4}$$

$$\rho\mathbf{u}(\mathbf{x},t) = m\int f(\mathbf{x},\mathbf{v},t)\mathbf{v}d\mathbf{v}. \tag{2.5}$$

In order to prove that Eq.(2.3) along with the definitions in Eqs.(2.4) and (2.5), are equivalent to Eqs.(2.1) and (2.2), we need to define an appropriate collision operator. Once we have defined a collision operator, we then use the Chapman-Enskog multi-scale expansion [25] to show the equivalence of these two approaches.

2.2 Binary and BGK Collision Operators

To complete Eq.(2.3), we must define a collision operator for the RHS. Under certain assumptions [24], we can consider only two-particle collisional effects where the most general form of the binary collision operator—often denoted by $Q(f,f)$—is

$$\left(\frac{df}{dt}\right)_c = Q(f,f) = \int\int[f(\mathbf{v}')f(\mathbf{v}_1') - f(\mathbf{v})f(\mathbf{v}_1)]\sigma d\Omega d\mathbf{v}_1. \tag{2.6}$$

The quantity $\sigma \equiv \sigma(|\mathbf{v}-\mathbf{v}_1|,\Omega)$ is the differential cross section for the collisions in which particles with incoming velocities $\mathbf{v}$ and $\mathbf{v_1}$ leave with velocities $\mathbf{v}'$ and $\mathbf{v_1'}$. Unfortunately, the generality of this collision operator makes it impossible to use directly; the Boltzmann equation becomes intractable if further simplification is not made. Before we proceed to replace this collision operator with a more practical one that reproduces the appropriate macroscopic behavior, we note a few key features of the general collision operator that we wish to reproduce in our approximation, or *model* collision operator.

First, the collision operator respects conservation of mass, momentum, and energy. This reflects the simple physical fact that particles which enter collisions do not leave

*We will use $\mathbf{u}$ for macroscopic (or mean) fluid velocities, reserving $\mathbf{v}$ for referencing microscopic, thermal particle velocities.

with excess energy, mass, or momentum. These constraints are expressed by the *collision invariants*

$$\psi_1(\mathbf{v}) = 1 \text{ (mass conservation)} \tag{2.7}$$

$$\psi_2(\mathbf{v}) = \mathbf{v} \text{ (momentum conservation)} \tag{2.8}$$

$$\psi_3(\mathbf{v}) = |\mathbf{v}|^2 \text{ (energy conservation)} \tag{2.9}$$

which are invariant in the sense that

$$\int Q(f,f)\psi_k(\mathbf{v})d\mathbf{v} = 0. \tag{2.10}$$

Second, we would like our collision operator to respect thermodynamic entropy laws. Boltzmann proved that $Q(f,f)$ respects the increasing entropy law by proving his famous H-theorem. If we define H as

$$H(t) = \int\int f \ln f d\mathbf{x}d\mathbf{v} \tag{2.11}$$

then it can be shown that

$$\frac{d}{dt}H(t) \leq 0 \tag{2.12}$$

when f evolves according to Eq.(2.3) equipped with the binary collision operator. The thermodynamic entropy of the distribution f is $-k_B H(t)$. Thus, if $H(t)$ is non-increasing, then the entropy is non-decreasing. The most interesting fact to come out of this is that $dH/dt = 0$ if and only if f is given by the classic Maxwellian distribution

$$f(\mathbf{x},\mathbf{v},t) = f^M(\mathbf{x},\mathbf{v},t) = n\left(\frac{1}{2\pi c_s^2}\right)^{D/2} \exp\left[-\frac{|\mathbf{v}-\mathbf{u}|^2}{2c_s^2}\right] \tag{2.13}$$

where D is the number of degrees of freedom in the problem, $c_s^2 \equiv k_B T/m$, and $\mathbf{u}$ is the mean velocity of the particles [24].

Bhatnagar, Gross, and Krook proposed the following model for the collision operator:

$$\left(\frac{df}{dt}\right)_c = -\frac{f(\mathbf{x},\mathbf{v},t) - f^{(eq)}(\mathbf{x},\mathbf{v},t)}{\tau_c} \tag{2.14}$$

where τ_c is proportional to the mean time between particle collisions and $f^{(eq)}$ is some equilibrium distribution to which particles tend to relax [1]. We can see that this collision operator has an intuitive feel as well: the distribution function f relaxes to some equilibrium distribution $f^{(eq)}$ at a rate proportional to its deviation from that equilibrium. With this collision operator, the Boltzmann equation becomes

$$\partial_t f(\mathbf{x},\mathbf{v},t) + \mathbf{v}\cdot\nabla f(\mathbf{x},\mathbf{v},t) = -\frac{f(\mathbf{x},\mathbf{v},t) - f^{(eq)}(\mathbf{x},\mathbf{v},t)}{\tau_c}. \tag{2.15}$$

To give insight into the relevant scales in this equation, we non-dimensionalize by making the following substitutions:

$$t = t_0\hat{t} \tag{2.16}$$

$$x = L_0\hat{\mathbf{x}} \tag{2.17}$$

$$\mathbf{v} = v_0\hat{\mathbf{v}} \tag{2.18}$$

$$f = f_0 F \tag{2.19}$$

$$\tau_c = \tau_0\hat{\tau_c}. \tag{2.20}$$

To maintain consistency in the units, we require

$$L_0 = v_0 t_0. \tag{2.21}$$

The result of these substitutions is:

$$\partial_{\hat{t}} F(\hat{\mathbf{x}},\hat{\mathbf{v}},\hat{t}) + \hat{\mathbf{v}}\cdot\hat{\nabla}F(\hat{\mathbf{x}},\hat{\mathbf{v}},\hat{t}) = -\frac{F(\hat{\mathbf{x}},\hat{\mathbf{v}},\hat{t}) - F^{(eq)}(\hat{\mathbf{x}},\hat{\mathbf{v}},\hat{t})}{\hat{\tau_c}\epsilon} \tag{2.22}$$

where $\epsilon = \tau_0/t_0$. The ratio ϵ is the Knudsen number. When $\epsilon \ll 1$, we can use it as the small parameter in a multi-scale expansion of the moments of Eq.(2.22). This procedure is called the Chapman-Enskog multi-scale expansion. If we take $f^{(eq)} = f^M$, the procedure produces the Navier-Stokes equations as given in Eqs.(2.1) and (2.2) with $\nu = \epsilon\tau_c c_s^2$ [24]. A third equation for the evolution of the internal energy of the fluid is also obtained; however, here we will consider isothermal closures as discussed before.

2.3 Discretizing the Boltzmann Equation

We proceed with the development of the LBM by discretizing Eq.(2.22), written here without the hats:

$$\partial_t F(\mathbf{x}, \mathbf{v}, t) + \mathbf{v} \cdot \nabla F(\mathbf{x}, \mathbf{v}, t) = -\frac{F(\mathbf{x}, \mathbf{v}, t) - F^{(eq)}(\mathbf{x}, \mathbf{v}, t)}{\tau_c \epsilon}. \tag{2.23}$$

Evidently, we must discretize this equation in velocity, space, and time. We begin by discretizing the velocity dimension, obtaining

$$\partial_t F_i(\mathbf{x}, t) + \mathbf{v}_i \cdot \nabla F_i(\mathbf{x}, t) = -\frac{F_i(\mathbf{x}, t) - F^{(eq)}(\mathbf{x}, t)}{\tau_c \epsilon} \tag{2.24}$$

where

$$F_i(\mathbf{x}, \mathbf{t}) \equiv F(\mathbf{x}, \mathbf{v}_i, \mathbf{t}) \tag{2.25}$$

and we have some discrete set of velocities $\mathbf{v}_i$. It will turn out that we need only a few velocities to reproduce the Navier-Stokes equations. Next we discretize Eq.(2.24) in space and time. We are faced with the standard set of choices for discretizing the spatial and temporal derivatives. Here we adopt the standard LBM discretization without further consideration for other possible discretizations. As we will see, the standard discretization results in a fully explicit upwind method that has second order accuracy both spatially and temporally on the Navier-Stokes equations. In one dimension, the

discretization looks like:

$$\begin{aligned}\frac{F_i(x,t+\delta t)-F_i(x,t)}{\delta t} &+ v_i\frac{F_i(x+\delta x_i,t+\delta t)-F_i(x,t+\delta t)}{\delta x_i}\\ &= -\frac{F_i(\mathbf{x},t)-F_i^{(eq)}(\mathbf{x},t)}{\tau_c\epsilon}.\end{aligned} \tag{2.26}$$

If we enforce

$$v_i = \frac{\delta x_i}{\delta t} \tag{2.27}$$

then we can rewrite Eq.(2.26) as:

$$F_i(x+v_i\delta t,t+\delta t)-F_i(x,t) = -\frac{\delta t}{\tau_c\epsilon}\left[F_i(x,t)-F_i^{(eq)}(x,t)\right]. \tag{2.28}$$

The multi-dimensional version is, analagously:

$$F_i(\mathbf{x}+\mathbf{v}_i\delta t,t+\delta t)-F_i(\mathbf{x},t) = -\frac{\delta t}{\tau_c\epsilon}\left[F_i(\mathbf{x},t)-F_i^{(eq)}(\mathbf{x},t)\right]. \tag{2.29}$$

The standard procedure then calls for identifying δt with ϵ, leading to

$$F_i(\mathbf{x}+\mathbf{v}_i\delta t,t+\delta t)-F_i(\mathbf{x},t) = -\frac{1}{\tau}\left[F_i(\mathbf{x},t)-F_i^{(eq)}(\mathbf{x},t)\right] \tag{2.30}$$

or

$$F_i(\mathbf{x}+\mathbf{v}_i\delta t,t+\delta t) = \left[1-\frac{1}{\tau}\right]F_i(\mathbf{x},t)+\left[\frac{1}{\tau}\right]F_i^{(eq)}(\mathbf{x},t) \tag{2.31}$$

where $\tau = \tau_c$ is the dimensionless relaxation parameter (we have dropped the subscipt to match standard notation). This equation suggests a very simple numerical implementation. At each time step, for each velocity $\mathbf{v}_i$, we form the sum on the RHS and then translate—or stream—the solution in the direction of $\mathbf{v}_i$. Now, because of the relation given in Eq.(2.27) the streaming step will be an integer number of grid cells, resulting in an efficient and easy to implement numerical scheme.

It is also interesting to note that enforcement of Eq.(2.27) is not necessary. In the case where Eq.(2.27) does not hold, the streaming step does not align with the spatial

grid, and one must implement interpolation algorithms to complete the streaming step. Relaxation of Eq.(2.27) may even lead to more stable numerical schemes by using the aditional flexibility to construct more isotropic sets of streaming vectors [19][16]. Here we will restrict ourselves to schemes where Eq.(2.27) is satisfied, and the streaming step does not require use of interpolation schemes.

2.4 Chapman-Enskog and Equilibrium Construction

To show that solving Eq.(2.31) does indeed reproduce Navier-Stokes equations, one applies a multi-scale Chapman-Enskog expansion using ϵ as the small parameter. If the Knudsen number ϵ is small, the standard Chapman-Enskog formalism calls for expanding F_i and ∂_t as

$$\begin{aligned} F_i = \sum_{n=0}^{\infty} \epsilon^n F_i^{(n)} &= F_i^{(0)} + \left[\epsilon F_i^{(1)} + \epsilon^2 F_i^{(2)} + ... \right] \\ &= F_i^{(eq)} + \left[F_i^{(neq)} \right] \end{aligned} \tag{2.32}$$

$$\partial_t = \sum_{n=0}^{\infty} \epsilon^n \partial_{t_n} = \partial_{t_0} + \epsilon \partial_{t_1} + ... \tag{2.33}$$

where we require that each of the the non-equilibrium parts do not contribute to the macroscopic field variables ρ and $\rho\mathbf{u}$:

$$\sum_i \epsilon^n F_i^{(n)} = 0 \quad \forall \quad n > 0 \tag{2.34}$$

$$\sum_i \mathbf{v}_i \epsilon^n F_i^{(n)} = \mathbf{0} \quad \forall \quad n > 0. \tag{2.35}$$

Recall that we identified the time step δt with the Knudsen number ϵ in our discrete equation. We therefore Taylor expand Eq.(2.31) in the small parameter δt. Keeping terms to order δt^2 from the Taylor expansion and making the multi-scale substitutions in Eqs.(2.32) and (2.33), we get

$$\left[\partial_{t_0} + \mathbf{v}_i \cdot \nabla \right] F_i^{(0)} = -\frac{F_i^{(1)}}{\tau} \tag{2.36}$$

$$\partial_{t_1} F_i^{(0)} + \left(1 - \frac{1}{2\tau}\right) \left[\partial_{t_0} + \mathbf{v}_i \cdot \nabla\right] F_i^{(1)} = -\frac{F_i^{(2)}}{\tau} \tag{2.37}$$

at the lowest two orders in ϵ (or δt). Taking the first and second moments of these will give equations for the evolution of ρ and $\rho\mathbf{u}$. As we will show later, the result is

$$\partial_t \sum_i F_i^{(0)} + \nabla \cdot (\sum_i \mathbf{v}_i F_i^{(0)}) = 0 \tag{2.38}$$

$$\partial_t (\sum_i \mathbf{v}_i F_i^{(0)}) + \nabla \cdot \left[\mathbf{\Pi}^{(0)} + \delta t \left(1 - \frac{1}{2\tau}\right) \mathbf{\Pi}^{(1)}\right] = O(\delta t^2) \tag{2.39}$$

where

$$\mathbf{\Pi}^{(0)} \equiv \sum_i \mathbf{v}_i \mathbf{v}_i F_i^{(0)} \tag{2.40}$$

$$\mathbf{\Pi}^{(1)} \equiv \sum_i \mathbf{v}_i \mathbf{v}_i F_i^{(1)} \tag{2.41}$$

The main work in developing a lattice kinetic scheme is then to find local equilibrium functions $F_i^{(0)}$ such that Eq.(2.39) gives the Navier-Stokes equation. To proceed towards this goal, it is necessary to define the form of $F_i^{(0)}$, along with a set of discrete velocities. The most commonly used set of velocities (also called streaming vectors) in 2D is the following:

$$\mathbf{v}_i = v \times \begin{cases} (0,0) & i = 0 \\ (\pm 1, 0), (0, \pm 1) & i = 1, 2, 3, 4 \\ (\pm 1, \pm 1) & i = 5, 6, 7, 8\,. \end{cases} \qquad \text{(D2Q9)} \tag{2.42}$$

This choice for the velocity discretization is the called the D2Q9 set, referencing the number of dimensions (two), and the number of streaming vectors (nine). This set owes its popularity to the fact that it has the minimum number of streaming vectors necessary to reproduce the isothermal Navier-Stokes equations on a square grid.*

*Actually, the zero velocity is not necessary; however, many authors have noted it has a very positive effect on the stability of the resultant numerical scheme.

The second necessary ingredient is an ansatz for $F_i^{(0)}$. The standard ansatz has the following form [4]:

$$F_i^{(0)} = \begin{cases} A_1 + B_1\mathbf{u}^2 + C_1(\mathbf{v}_i\cdot\mathbf{u}) + D_1(\mathbf{v}_i\cdot\mathbf{u})^2 & i = 0 \\ A_2 + B_2\mathbf{u}^2 + C_2(\mathbf{v}_i\cdot\mathbf{u}) + D_2(\mathbf{v}_i\cdot\mathbf{u})^2 & i = 1,2,3,4 \\ A_3 + B_3\mathbf{u}^2 + C_3(\mathbf{v}_i\cdot\mathbf{u}) + D_3(\mathbf{v}_i\cdot\mathbf{u})^2 & i = 5,6,7,8\,. \end{cases} \tag{2.43}$$

The resultant scheme for this ansatz is

$$F_i^{(0)} = \begin{cases} \frac{16}{36}\rho\left[1 - \frac{3}{2}\mathbf{u}^2 + 3(\mathbf{v}_i\cdot\mathbf{u}) + \frac{9}{2}(\mathbf{v}_i\cdot\mathbf{u})^2\right] & i = 0 \\ \frac{4}{36}\rho\left[1 - \frac{3}{2}\mathbf{u}^2 + 3(\mathbf{v}_i\cdot\mathbf{u}) + \frac{9}{2}(\mathbf{v}_i\cdot\mathbf{u})^2\right] & i = 1,2,3,4 \\ \frac{1}{36}\rho\left[1 - \frac{3}{2}\mathbf{u}^2 + 3(\mathbf{v}_i\cdot\mathbf{u}) + \frac{9}{2}(\mathbf{v}_i\cdot\mathbf{u})^2\right] & i = 5,6,7,8 \end{cases} \tag{2.44}$$

for streaming vector length $v = 1$. The resulting equations (i.e. the zeroth and first moments of Eqs.(2.36) and (2.37)) with this equilibrium are [13]

$$\partial_{t_0}\rho + \nabla\cdot(\rho\mathbf{u}) = 0 \tag{2.45}$$

$$\partial_{t_1}\rho = 0 \tag{2.46}$$

$$\partial_{t_0}(\rho\mathbf{u}) + \nabla\cdot(\rho\mathbf{u}\mathbf{u}) + \nabla(c_s^2\rho) = 0 \tag{2.47}$$

$$\partial_{t_1}\rho + \nabla\cdot\left(2\nu\rho\mathbf{S} - \delta t\left(\tau - \frac{1}{2}\right)\nabla\cdot(\rho\mathbf{u}\mathbf{u}\mathbf{u})\right) = 0 \tag{2.48}$$

with

$$\mathbf{S} = \frac{1}{2}\left[\nabla\mathbf{u} + (\nabla\mathbf{u})^{\mathrm{T}}\right] \tag{2.49}$$

$$\nu = \frac{1}{6}\left[2\tau - 1\right]\delta t. \tag{2.50}$$

In the incompressible limit, when $\nabla\cdot\mathbf{u} = 0$ and $\nabla\rho = 0$, these equations are equivalent to Eqs.(2.1) and (2.2) because the $\nabla\cdot(\rho\mathbf{u}\mathbf{u}\mathbf{u})$ term becomes negligible. Thus, using the D2Q9 velocity distribution and the ansatz in Eq.(2.43), we can construct a scheme

that is consistent with the incompressible Navier-Stokes equations. One can eliminate this spurious $\nabla \cdot (\rho \mathbf{uuu})$ term by extending the ansatz to include higher powers of $\mathbf{u}$; however, this has the drawback of requiring additional streaming vectors [9].

It has been observed that the equilibrium distribution in Eq.(2.44) can also be arrived at by Taylor expanding the Maxwellian distribution f^M in small Mach number $\text{Ma} \equiv \frac{|\mathbf{u}|}{c_s}$ and then using a Gaussian quadrature on the $F_i^{(0)}$ to enforce the moment constraints [15]. The Taylor expansion of f^M gives rise to

$$\left[1 - \frac{3}{2}\mathbf{u}^2 + 3(\mathbf{v}_i \cdot \mathbf{u}) + \frac{9}{2}(\mathbf{v}_i \cdot \mathbf{u})^2\right] \tag{2.51}$$

while the differing weights in Eq.(2.44) arise from the quadrature.

For the present work, we will follow the procedure outlined in the appendix of [13] to construct a 3D lattice kinetic scheme to solve the resistive MHD equations. In order to recover the 3D equations, we will use the following, D3Q19, set of streaming vectors:

$$\mathbf{v}_i = v \times \begin{cases} (0,0,0) & i = 0 \\ (\pm 1,0,0),(0,\pm 1,0),(0,0,\pm 1) & i = 1,...,6 \\ (\pm 1,\pm 1,0),(\pm 1,0,\pm 1),(0,\pm 1,\pm 1) & i = 7,...,18\ . \end{cases} \tag{2.52}$$

In our case the moments of Eqs.(2.36) and (2.37) will force the introduction of terms involving $\mathbf{B}$ into $F_i^{(0)}$. Our ansatz will be of the form:

$$F_i^{(0)} = \begin{cases} A_1 + B_1\mathbf{u}^2 + C_1\mathbf{B}^2 & i = 0 \\ A_2 + B_2\mathbf{u}^2 + C_2\mathbf{B}^2 + D_1(\mathbf{v}_i \cdot \mathbf{u}) + E_1(\mathbf{v}_i \cdot \mathbf{u})^2 + F_1(\mathbf{v}_i \cdot \mathbf{B})^2 & i = 1,...,6 \\ A_3 + B_3\mathbf{u}^2 + C_3\mathbf{B}^2 + D_2(\mathbf{v}_i \cdot \mathbf{u}) + E_2(\mathbf{v}_i \cdot \mathbf{u})^2 + F_2(\mathbf{v}_i \cdot \mathbf{B})^2 & i = 7,...,18 \end{cases} \tag{2.53}$$

where we have abused notion in our choice of B as both a coefficient and the magnetic field. It will always be clear from context whether we are referring to the coefficient or the magnetic field. In the next chapter we will proceed to derive the appropriate coefficients for the ansatz and also treat the magnetic field $\mathbf{B}$ within the lattice kinetic framework. The resulting scheme is the 3D analog of the 2D scheme derived in [9].

Chapter 3
Derivation of a LBM for 3D MHD

In this chapter we derive the equilibrium functions for our 3D lattice kinetic scheme. Before proceeding to this, we first present a derivation of the resistive MHD equations which they will model. Just as there is more than one way of arriving at the Navier-Stokes equations, there is more than one way of arriving at the MHD equations. We choose to derive them systematically from moments of the Boltzmann equation with a Lorentz term. This approach is more in the spirit of kinetic theory than a phenomenological approach. Different instances of this derivation may also be found in standard plasma physics texts. For example, we borrow the begining of what follows from [23].

3.1 Single-Fluid Resistive MHD Equations

In general, a plasma contains many ion species along with electrons, each described by its own distribution f with a corresponding Boltzmann equation. The MHD approximation assumes a one-species plasma in which case the plasma may be characterized by an ion distribution f_i and an electron distribution f_e. MHD also restricts itself to fully ionized and neutral plasmas; later, this assumption will allow us to reduce the two-fluid system resulting from f_i and f_e to a single-fluid system. To close the resistive MHD system, Maxwell's equations will be included to describe the evolution of the electromagnetic fields embedded in the plasma. We will non-dimensionalize the system and then discuss which terms are neglected in resistive MHD.

For each of the species, we start with the Boltzmann equation

$$\partial_t f + \mathbf{v} \cdot \nabla f + \frac{q}{m} \left[\mathbf{E} + \mathbf{v} \times \mathbf{B} \right] \cdot \nabla_{\mathbf{v}} f = \left(\frac{\partial f}{\partial t} \right)_c \tag{3.1}$$

where $\mathbf{F}$ has been replaced by the Lorentz force, $q\left[\mathbf{E} + \mathbf{v} \times \mathbf{B}\right]$. The $\mathbf{F}$ may include other forces such as gravity; however, for this treatment we will retain only the Lorentz

force. This equation applies to both the ion distribution f_i and the electron distribution f_e. As we proceed, f will be used with the implication that there are actually two Boltzmann equations, one for f_i and one for f_e. Recall that zeroth and first moments of the Boltzmann equation give the continuity and momentum equations. To recover the continuity equation, we take the zeroth moment of Eq.(3.1):

$$\int \partial_t f d\mathbf{v} + \int \mathbf{v} \cdot \nabla f d\mathbf{v} + \int \frac{q}{m} \left[\mathbf{E} + \mathbf{v} \times \mathbf{B}\right] \cdot \nabla_{\mathbf{v}} f d\mathbf{v} = \int \left(\frac{\partial f}{\partial t}\right)_c d\mathbf{v}. \tag{3.2}$$

The RHS is zero by conservation of mass. The force due to $\mathbf{E}$ in the Lorentz term on the LHS can be rewritten using the divergence theorem as a surface integral over the surface of the phase space where $\|\mathbf{v}\| = \infty$.

$$\int \mathbf{E} \cdot \nabla_{\mathbf{v}} f d\mathbf{v} = \int_{\|\mathbf{v}\|=\infty} f\mathbf{E} \cdot d\mathbf{A} = 0. \tag{3.3}$$

This integral is taken over the surface where $\|\mathbf{v}\| = \infty$ and must be 0 if the system has finite energy. The $\mathbf{v} \times \mathbf{B}$ force in the Lorentz term can be rewritten using basic vector identities and the divergence theorem as

$$\int (\mathbf{v} \times \mathbf{B}) \cdot \nabla_{\mathbf{v}} f d\mathbf{v} = \int_{\|\mathbf{v}\|=\infty} (f\mathbf{v} \times \mathbf{B}) \cdot d\mathbf{A} - \int f \nabla_{\mathbf{v}} \times (\mathbf{v} \times \mathbf{B}) d\mathbf{v} \tag{3.4}$$

where the first integral again zero for distributions with finite energy. The remaining terms are simplified using definitions of n and $\mathbf{u}$ to get

$$\partial_t n + \nabla \cdot (n\mathbf{u}) = 0. \tag{3.5}$$

Multiplying by the mass m of the particles gives

$$\partial_t \rho + \nabla \cdot (\rho\mathbf{u}) = 0. \tag{3.6}$$

To recover the momentum equation, we take the first moment of Eq.(3.1):

$$\int \partial_t f \mathbf{v} d\mathbf{v} + \int \mathbf{v} \cdot \nabla f \mathbf{v} d\mathbf{v} + \int \frac{q}{m} \left[\mathbf{E} + \mathbf{v} \times \mathbf{B}\right] \cdot \nabla_{\mathbf{v}} f \mathbf{v} d\mathbf{v} = \int \left(\frac{\partial f}{\partial t}\right)_c \mathbf{v} d\mathbf{v}. \tag{3.7}$$

The second term can be written as

$$\nabla \cdot \int f \mathbf{v}\mathbf{v} d\mathbf{v} = \nabla \cdot \int f(\mathbf{u}+\tilde{\mathbf{v}})^2 d\mathbf{v} = \nabla \cdot \int f(\mathbf{u}\mathbf{u}+\tilde{\mathbf{v}}\tilde{\mathbf{v}}+2\mathbf{u}\tilde{\mathbf{v}}) d\mathbf{v} \tag{3.8}$$

using $\tilde{\mathbf{v}}$ as the microscopic particle velocity so that $\mathbf{v} = \mathbf{u} + \tilde{\mathbf{v}}$. Since the mean of the random microscopic velocity fluctuations $\tilde{\mathbf{v}}$ is zero by definition, this expression reduces to

$$\nabla \cdot \int f(\mathbf{u}\mathbf{u}+\tilde{\mathbf{v}}\tilde{\mathbf{v}}+2\mathbf{u}\tilde{\mathbf{v}}) d\mathbf{v} = \nabla \cdot (n\mathbf{u}\mathbf{u} + n\overline{\tilde{\mathbf{v}}\tilde{\mathbf{v}}}) \tag{3.9}$$

where second term in this expression is the definition of stress tensor $\mathbf{P}/m$. Algebra, along with the finite energy argument used previously, gives us the following for the third term in Eq.(3.7):

$$\int \frac{q}{m} \left[\mathbf{E} + \mathbf{v} \times \mathbf{B}\right] \cdot \nabla_{\mathbf{v}} f \mathbf{v} d\mathbf{v} = -\frac{qn}{m} \left[\mathbf{E} + \mathbf{u} \times \mathbf{B}\right]. \tag{3.10}$$

The final simplification of Eq.(3.7) is

$$\partial_t (n\mathbf{u}) + \nabla \cdot (n\mathbf{u}\mathbf{u}) + \nabla \cdot \frac{\mathbf{P}}{m} - \frac{qn}{m} \left[\mathbf{E} + \mathbf{u} \times \mathbf{B}\right] = \int \left(\frac{\partial f}{\partial t}\right)_c \mathbf{v} d\mathbf{v}. \tag{3.11}$$

Multiplying by the particle mass m this equation is:

$$\partial_t (\rho\mathbf{u}) + \nabla \cdot (\rho\mathbf{u}\mathbf{u}) + \nabla \cdot \mathbf{P} - qn \left[\mathbf{E} + \mathbf{u} \times \mathbf{B}\right] = \int \left(\frac{\partial f}{\partial t}\right)_c m\mathbf{v} d\mathbf{v}. \tag{3.12}$$

In conclusion, we have the following equations:

$$\partial_t \rho_i + \nabla \cdot (\rho_i \mathbf{u}_i) = 0 \tag{3.13}$$

$$\partial_t \rho_e + \nabla \cdot (\rho_e \mathbf{u}_e) = 0 \tag{3.14}$$

$$\partial_t (\rho_i \mathbf{u}_i) + \nabla \cdot (\rho_i \mathbf{u}_i \mathbf{u}_i) + \nabla \cdot \mathbf{P}_i - e n_i \left[\mathbf{E} + \mathbf{u}_i \times \mathbf{B}\right] = M_i \int \left(\frac{\partial f_i}{\partial t}\right)_c \mathbf{v} d\mathbf{v} \tag{3.15}$$

$$\partial_t (\rho_e \mathbf{u}_e) + \nabla \cdot (\rho_e \mathbf{u}_e \mathbf{u}_e) + \nabla \cdot \mathbf{P}_e + e n_e \left[\mathbf{E} + \mathbf{u}_e \times \mathbf{B}\right] = m_e \int \left(\frac{\partial f_e}{\partial t}\right)_c \mathbf{v} d\mathbf{v}. \tag{3.16}$$

The collision terms, which are non-zero due to electron-ion collisions, can be computed as [23]:

$$m_e \int \left(\frac{\partial f_e}{\partial t}\right)_c \mathbf{v} d\mathbf{v} = \eta e^2 n^2 (\mathbf{u}_i - \mathbf{u}_e) \tag{3.17}$$

for the electron equation and

$$M_i \int \left(\frac{\partial f_i}{\partial t}\right)_c \mathbf{v} d\mathbf{v} = -m_e \int \left(\frac{\partial f_e}{\partial t}\right)_c \mathbf{v} d\mathbf{v} = \eta e^2 n^2 (\mathbf{u}_e - \mathbf{u}_i) \tag{3.18}$$

for the ion equation. We use $n = n_e = n_i$ by invoking the plasma neutrality assumption. Thus, the momentum equations become

$$\partial_t(\rho_i \mathbf{u}_i) + \nabla \cdot (\rho_i \mathbf{u}_i \mathbf{u}_i) + \nabla \cdot \mathbf{P}_i - e n_i \left[\mathbf{E} + \mathbf{u}_i \times \mathbf{B}\right] = \eta e^2 n^2 (\mathbf{u}_i - \mathbf{u}_e) \tag{3.19}$$

$$\partial_t(\rho_e \mathbf{u}_e) + \nabla \cdot (\rho_e \mathbf{u}_e \mathbf{u}_e) + \nabla \cdot \mathbf{P}_e + e n_e \left[\mathbf{E} + \mathbf{u}_e \times \mathbf{B}\right] = \eta e^2 n^2 (\mathbf{u}_e - \mathbf{u}_i). \tag{3.20}$$

Eqs.(3.13), (3.14), (3.19), and (3.20) describe a two fluid system: one fluid being ions, one fluid being the electrons. We can transform these equations into a one-fluid system by taking four specific linear combinations of these equations and applying the following definitions:

$$\rho \equiv \rho_i + \rho_e \tag{3.21}$$

$$M \equiv M_i + m_e \tag{3.22}$$

$$\rho \mathbf{u} \equiv \rho_i \mathbf{u}_i + \rho_e \mathbf{u}_e \tag{3.23}$$

$$\mathbf{P} \equiv \mathbf{P}_i + \mathbf{P}_e \tag{3.24}$$

$$\mathbf{J} \equiv e n (\mathbf{u}_i - \mathbf{u}_e). \tag{3.25}$$

The sum of Eqs.(3.13) and (3.14) gives, using Eqs.(3.21) thru (3.25),

$$\partial_t \rho + \nabla \cdot \rho \mathbf{u} = 0. \tag{3.26}$$

Subtracting Eqs.(3.13) and (3.14), after dividing each equation by its respective particle mass, gives

$$\nabla \cdot \mathbf{J} = 0. \tag{3.27}$$

The sum of Eqs.(3.19) and (3.20) gives

$$\partial_t(\rho\mathbf{u}) + \nabla \cdot (\rho\mathbf{u}\mathbf{u}) + \frac{M_i m_e}{e^2}\nabla \cdot \left(\frac{\mathbf{J}\mathbf{J}}{\rho}\right) + \nabla \cdot \mathbf{P} - \mathbf{J} \times \mathbf{B} = 0 \tag{3.28}$$

where we have used the approximation

$$\mathbf{u}_i = \mathbf{u} + \frac{m_e}{M_i}\frac{\mathbf{J}}{ne} \approx \mathbf{u} \tag{3.29}$$

on the basis that ion mass is thousands of times greater than the electron mass (i.e. $M_i \gg m_e$). Finally, adding Eqs.(3.19) and (3.20) after multiplying each by its respective charge-to-mass ratio q/m gives

$$\mathbf{E} + \mathbf{u} \times \mathbf{B} = \frac{m_e M_i}{e^2\rho}\left[\partial_t \mathbf{J} + \nabla \cdot (\mathbf{u}\mathbf{J} + \mathbf{J}\mathbf{u})\right] - \frac{M}{e\rho}\nabla \cdot \mathbf{P}_e + \frac{M_i}{e\rho}(\mathbf{J} \times \mathbf{B}) + \eta\mathbf{J}. \tag{3.30}$$

Collecting the four linear combinations of the four two-fluid equations results in an equivalent (up to approximation) new set of single fluid equations

$$\nabla \cdot \mathbf{J} = 0 \tag{3.31}$$

$$\partial_t \rho + \nabla \cdot \rho\mathbf{u} = 0 \tag{3.32}$$

$$\partial_t(\rho\mathbf{u}) + \nabla \cdot (\rho\mathbf{u}\mathbf{u}) + \frac{M_i m_e}{e^2}\nabla \cdot \left(\frac{\mathbf{J}\mathbf{J}}{\rho}\right) - \nabla \cdot \mathbf{P} + \mathbf{J} \times \mathbf{B} = 0 \tag{3.33}$$

$$\mathbf{E} + \mathbf{u} \times \mathbf{B} = \frac{m_e M_i}{e^2\rho}\left[\partial_t \mathbf{J} + \nabla \cdot (\mathbf{u}\mathbf{J} + \mathbf{J}\mathbf{u})\right] - \frac{M}{e\rho}\nabla \cdot \mathbf{P}_e + \frac{M_i}{e\rho}(\mathbf{J} \times \mathbf{B}) + \eta\mathbf{J}. \tag{3.34}$$

To close this system we need Maxwell's equations

$$\nabla \times \mathbf{E} \;=\; -\partial_t \mathbf{B} \tag{3.35}$$

$$\nabla \times \mathbf{B} = \frac{1}{c^2}\partial_t \mathbf{E} + \mu_0 \mathbf{J} \tag{3.36}$$

$$\nabla \cdot \mathbf{B} = 0 \tag{3.37}$$

$$\nabla \cdot \mathbf{E} = 0 \tag{3.38}$$

for the evolution of the electric and magnetic fields.* We will also disregard the displacement current $\frac{1}{c^2}\partial_t \mathbf{E}$ because its only relevant when plasma velocities approach c. Finally, we will take the isothermal approximation for this work, so that the scalar part of the pressure tensor is $p = p_i + p_e = nk_B(T_e + T_i) = \frac{k_B T}{m}\rho$ where we have defined $T = T_e + T_i$.† We will take the entire pressure tensor to be

$$\mathbf{P} = p\mathbf{I} - 2\nu\rho\mathbf{S}. \tag{3.39}$$

The off-diagonal parts of the pressure tensor are described by $\mathbf{S}$. These off diagonal components are generally included in resistive MHD in the form of an $\nu\rho\nabla^2\mathbf{u}$ term in the momentum equation. In the Navier-Stokes equations $\mathbf{S}$ is non-zero when the distribution function f departs from a Maxwellian. In any event, we adopt this form because this is the form that will later arise from the Chapman-Enskog multi-scale expansion.

Next, we non-dimensionalize the equations derived in the last section and discuss the regime referred to as MHD. Non-dimensionalization proceeds by replacing the fundamental quantities $\mathbf{E}$, $\mathbf{B}$, $\mathbf{u}$, ρ with $\hat{\mathbf{E}}$, $\hat{\mathbf{B}}$, $\hat{\mathbf{u}}$, $\hat{\rho}$ where

$$\mathbf{E} = E_0\hat{\mathbf{E}} \tag{3.40}$$

$$\mathbf{B} = B_0\hat{\mathbf{B}} \tag{3.41}$$

$$\mathbf{u} = u_0\hat{\mathbf{u}} \tag{3.42}$$

$$\rho = \rho_0\hat{\rho}. \tag{3.43}$$

*$\nabla \cdot \mathbf{E} = 0$ because we have assumed the plasma is neutral. Also, the last two equations are implied by the first two if they are satisfied by the initial conditions.

†We will continue to define $c_s^2 \equiv \frac{k_B T}{m}$.

The subscripted quantities carry units, and thus the hatted variables are unitless. We also rescale the domain over which these variables are defined by making similar substitutions:

$$t = t_0\hat{t} \tag{3.44}$$

$$x = L_0\hat{x}. \tag{3.45}$$

To preserve units, the following relationships between unit-ed quantities must hold:

$$E_0 \equiv u_0 B_0 \tag{3.46}$$

$$u_0 \equiv \frac{B_0}{\mu_0\rho_0} \tag{3.47}$$

$$t_0 \equiv \frac{L_0}{u_0}. \tag{3.48}$$

In this process, the non-fundamental quantities such as $\mathbf{P}$, $\mathbf{J}$ will also be renormalized as follows:

$$p = P_0\hat{p} \text{ and } \mathbf{P} = P_0\hat{\mathbf{P}} \quad \text{with} \quad P_0 = \frac{B_0^2}{\mu_0} \tag{3.49}$$

$$\mathbf{J} = J_0\hat{\mathbf{J}} \quad \text{with} \quad J_0 = \frac{B_0}{\mu_0 L_0}. \tag{3.50}$$

We begin by making these substitutions into Eq.(3.34) resulting in:

$$\begin{aligned}\hat{\mathbf{E}} + \hat{\mathbf{u}} \times \hat{\mathbf{B}} = & \left(\frac{c/\omega_{pe}}{L_0}\right)^2 \frac{1}{\hat{\rho}}\left[\partial_{\hat{t}}\hat{\mathbf{J}} + \nabla\cdot(\hat{\mathbf{u}}\hat{\mathbf{J}} + \hat{\mathbf{J}}\hat{\mathbf{u}})\right] \\ - & \left(\frac{c/\omega_{pi}}{L_0}\right)\frac{1}{\hat{\rho}}\nabla\cdot\hat{\mathbf{P}}_e \\ + & \left(\frac{c/\omega_{pi}}{L_0}\right)\frac{1}{\hat{\rho}}(\hat{\mathbf{J}}\times\hat{\mathbf{B}}) \\ + & \left(\frac{\eta}{L_0 u_0 \mu_0}\right)\hat{\mathbf{J}}\end{aligned} \tag{3.51}$$

where we have made use of the electon and ion plasma frequencies

$$\omega_{pe} = \sqrt{\frac{n_0 e^2}{\epsilon_0 m_e}} \tag{3.52}$$

$$\omega_{pi} = \sqrt{\frac{n_0 e^2}{\epsilon_0 M_i}}. \tag{3.53}$$

For ideal MHD, the entire RHS of Eq.(3.51) is assumed small. Keeping the last term results in resistive MHD. Keeping the next to last term results in Hall MHD. For now, we are interested in simulating regimes where all but the last term can be neglected, resulting in:

$$\hat{\mathbf{E}} + \hat{\mathbf{u}} \times \hat{\mathbf{B}} = \left(\frac{\eta}{L_0 u_0 \mu_0} \right) \hat{\mathbf{J}}. \tag{3.54}$$

Performing the same non-dimensionalization on Eq.(3.32), we get

$$\partial_{\hat{t}}(\hat{\rho}\hat{\mathbf{u}}) + \hat{\nabla}(\hat{\rho}\hat{\mathbf{u}}\hat{\mathbf{u}}) + \left(\frac{c/\omega_{pe}}{L_0} \right)^2 \hat{\nabla} \cdot \left(\frac{\hat{\mathbf{J}}\hat{\mathbf{J}}}{\hat{\rho}} \right) + \hat{\nabla}\hat{p} - \left(\frac{\nu}{u_0 L_0} \right) \hat{\nabla} \cdot (2\hat{\rho}\hat{\mathbf{S}}) - \hat{\mathbf{J}} \times \hat{\mathbf{B}} = 0 \tag{3.55}$$

where we will assume the third term is small for the same reason we assumed the first term of Eq.(3.51) was small. Finally, for Eq.(3.31) non-dimensionalization gives:

$$\partial_{\hat{t}}\hat{\rho} + \hat{\nabla} \cdot (\hat{\rho}\hat{\mathbf{u}}) = 0. \tag{3.56}$$

Non-dimensionalizing the two relevant Maxwell equations—having neglected the displacement current—we get

$$\hat{\nabla} \times \hat{\mathbf{E}} = -\partial_{\hat{t}}\hat{\mathbf{B}} \tag{3.57}$$

$$\hat{\nabla} \times \hat{\mathbf{B}} = \hat{\mathbf{J}} \tag{3.58}$$

In summary, the non-dimensionalized equations are, neglecting terms which are small in the MHD regime we are examining,

$$\partial_{\hat{t}}\hat{\rho} + \hat{\nabla} \cdot (\hat{\rho}\hat{\mathbf{u}}) = 0 \tag{3.59}$$

$$\partial_{\hat{t}}(\hat{\rho}\hat{\mathbf{u}}) + \hat{\nabla}(\hat{\rho}\hat{\mathbf{u}}\hat{\mathbf{u}}) + \hat{\nabla}\hat{p} - \hat{\mathbf{J}} \times \hat{\mathbf{B}} = \left(\frac{\nu}{u_0 L_0}\right) \hat{\nabla} \cdot (2\hat{\rho}\hat{\mathbf{S}}) \tag{3.60}$$

$$\hat{\mathbf{E}} + \hat{\mathbf{u}} \times \hat{\mathbf{B}} = \left(\frac{\eta}{L_0 u_0 \mu_0}\right) \hat{\mathbf{J}} \tag{3.61}$$

$$\hat{\nabla} \times \hat{\mathbf{E}} = -\partial_{\hat{t}} \hat{\mathbf{B}} \tag{3.62}$$

$$\hat{\nabla} \times \hat{\mathbf{B}} = \hat{\mathbf{J}}. \tag{3.63}$$

The reader may recognize the dimensionless Reynolds (Re) and magnetic Reynolds (Rm) numbers in the above equations:

$$\frac{1}{\mathrm{Re}} = \frac{\nu}{u_0 L_0} \tag{3.64}$$

$$\frac{1}{\mathrm{Rm}} = \frac{\eta}{L_0 u_0 \mu_0}. \tag{3.65}$$

Using these definitions and eliminating $\mathbf{E}$ and $\mathbf{J}$, we can rewrite the equations as:

$$\partial_t \rho + \nabla \cdot (\rho \mathbf{u}) = 0 \tag{3.66}$$

$$\partial_t(\rho\mathbf{u}) + \nabla(\rho\mathbf{u}\mathbf{u}) + \nabla p - (\nabla \times \mathbf{B}) \times \mathbf{B} = \frac{1}{\mathrm{Re}} \hat{\nabla} \cdot (2\hat{\rho}\hat{\mathbf{S}}) \tag{3.67}$$

$$\nabla \times (\frac{1}{\mathrm{Rm}} \nabla \times \mathbf{B} - \mathbf{u} \times \mathbf{B}) = -\partial_t \mathbf{B} \tag{3.68}$$

where we have dropped the hats.

3.2 D3Q19 Lattice Kinetic Scheme

The next step is to develop a lattice Boltzmann scheme that will recover the equations derived in the previous section. Clearly the added complication over a purely hydrodynamic system is that we must treat the magnetic field $\mathbf{B}$ in addition to the fluid. In order to realize the main advantages of the lattice Boltzmann schemes outlined in the introduction, we must treat the magnetic field analogously to the fluid fields; that is, $\mathbf{B}$ must be recovered from the moment of some distribution function that evolves according to a Boltzmann equation.

To get an idea of the type of distribution function we will need, lets begin by considering the ideal MHD equations. We use the condition that $\nabla \cdot \mathbf{B} = 0$ to rewrite the MHD equations in conservative form:

$$\begin{aligned} \partial_t \rho + \nabla \cdot (\rho \mathbf{u}) &= 0 && (3.69) \\ \partial_t (\rho \mathbf{u}) + \nabla \cdot \left[\rho \mathbf{u}\mathbf{u} + \left(p + \frac{B^2}{2} \right) \mathbf{I} - \mathbf{B}\mathbf{B} \right] &= 0 && (3.70) \\ \partial_t \mathbf{B} + \nabla \cdot (\mathbf{u}\mathbf{B} - \mathbf{B}\mathbf{u}) &= 0 && (3.71) \end{aligned}$$

or, using tensor notation, *

$$\begin{aligned} \partial_t \rho + \partial_\beta (\rho u_\alpha) &= 0 && (3.72) \\ \partial_t (\rho u_\alpha) + \partial_\beta \left[\rho u_\alpha u_\beta + \left(p + \frac{B^2}{2} \right) \delta_{\alpha\beta} - B_\alpha B_\beta \right] &= 0 && (3.73) \\ \partial_t B_\alpha + \partial_\beta \left(u_\alpha B_\beta - B_\alpha u_\beta \right) &= 0. && (3.74) \end{aligned}$$

If we make the following definitions:

$$\begin{aligned} \Pi_{\alpha\beta} &\equiv \rho u_\alpha u_\beta + \left(p + \frac{B^2}{2} \right) \delta_{\alpha\beta} - B_\alpha B_\beta && (3.75) \\ \Lambda_{\alpha\beta} &\equiv u_\alpha B_\beta - B_\alpha u_\beta && (3.76) \end{aligned}$$

these equations can be written as

$$\begin{aligned} \partial_t \rho + \partial_\beta (\rho u_\alpha) &= 0 && (3.77) \\ \partial_t (\rho u_\alpha) + \partial_\beta \Pi_{\alpha\beta} &= 0 && (3.78) \\ \partial_t B_\alpha + \partial_\beta \Lambda_{\alpha\beta} &= 0. && (3.79) \end{aligned}$$

The expressions being operated on by the divergence operator are the momentum flux ($\Pi_{\alpha\beta}$) and magnetic flux ($\Lambda_{\alpha\beta}$) tensors. For the fluid, the momentum flux tensor $\Pi_{\alpha\beta}$

*Where repeated indices will imply summation unless otherwise noted.

arises as the second moment of the distribution function f:

$$\rho = m\int f d\mathbf{v} \tag{3.80}$$

$$\rho u_\alpha = m\int f v_\alpha d\mathbf{v} \tag{3.81}$$

$$\Pi_{\alpha\beta} = m\int f v_\alpha v_\beta d\mathbf{v}. \tag{3.82}$$

Ideally, we would like to recover $\mathbf{B}$ and $\Lambda_{\alpha\beta}$ from a similar hierarchy of moments of a distribution function g

$$B_\alpha \stackrel{?}{=} \int g v_\alpha d\mathbf{v} \tag{3.83}$$

$$\Lambda_{\alpha\beta} \stackrel{?}{=} \int g v_\alpha v_\beta d\mathbf{v} \tag{3.84}$$

where now $\mathbf{v}$ is velocity of some fictitious particle whose existence is not physical but is only used to model the induction MHD equation. A quick examination reveals that this approach is bound to fail because the RHS of Eq.(3.84) is symmetric while the LHS, given in Eq.(3.76), is anti-symmetric. Because $\Lambda_{\alpha\beta}$ is anti-symmetric, we will have to approach the magnetic field variables in a fundamentally different way from the fluid variables.

There are two approaches to defining a set of distribution functions that allow the recovery of $\mathbf{B}$. One approach is through the bi-directional streaming model of Chen, et al.[6]. This approach has many drawbacks relative to the method we use in the present work. The primary disadvantage is that the resistivity η and viscosity ν cannot be set independently[17]. A second approach, proposed by Dellar[9], recovers each component of $\mathbf{B}$ from its own distribution function. The result is a vector-valued distribution function g_α where

$$B_\alpha = \int g_\alpha(\mathbf{x},\mathbf{v},t) d\mathbf{v} \tag{3.85}$$

$$\Lambda_{\alpha\beta} = \int v_\alpha g_\beta(\mathbf{x},\mathbf{v},t) d\mathbf{v}. \tag{3.86}$$

The hope is we can construct a $g_\alpha^{(eq)}$ such that when g_α evolves according to the standard BGK Boltzmann equation

$$\partial_t g_\alpha + \mathbf{v} \cdot \nabla g_\alpha = \frac{g_\alpha - g_\alpha^{(eq)}}{\tau_m} \tag{3.87}$$

we recover the appropriate macroscopic behavior for the magnetic field.

We proceed then with the goal of constructing the equilibrium distribution functions $F_i^{(eq)}$ and $G_{\alpha i}^{(eq)}$ such that when F_i and $G_{\alpha i}$ evolve according to

$$F_i(\mathbf{x} + \mathbf{v}_i \delta t, t + \delta t) = \left[1 - \frac{1}{\tau_f}\right] F_i(\mathbf{x}, t) + \left[\frac{1}{\tau_f}\right] F_i^{(eq)}(\mathbf{x}, t) \tag{3.88}$$

$$G_{\alpha i}(\mathbf{x} + \mathbf{v}_i \delta t, t + \delta t) = \left[1 - \frac{1}{\tau_g}\right] G_{\alpha i}(\mathbf{x}, t) + \left[\frac{1}{\tau_g}\right] G_{\alpha i}^{(eq)}(\mathbf{x}, t) \tag{3.89}$$

we recover the correct macroscopic MHD equations. Recall that we can use the Chapman-Enskog multi-scale expansion on these equations to get

$$\left[\partial_{t_0} + \mathbf{v}_i \cdot \nabla\right] F_i^{(0)} = -\frac{F_i^{(1)}}{\tau_f} \tag{3.90}$$

$$\partial_{t_1} F_i^{(0)} + \left(1 - \frac{1}{2\tau}\right) \left[\partial_{t_0} + \mathbf{v}_i \cdot \nabla\right] F_i^{(1)} = -\frac{F_i^{(2)}}{\tau_f} \tag{3.91}$$

at the lowest two orders in ϵ. There is a corresponding set for $G_{\alpha i}$. If we take the moments of these two equations, we will recover the macroscopic equations that are being solved by this numerical method. Taking the zeroth and first moments of the lowest order equation in ϵ, we get

$$\partial_{t_0} \sum_i F_i^{(0)} + \sum_i \mathbf{v}_i \cdot \nabla F_i^{(0)} = -\frac{1}{\tau_f} \sum_i F_i^{(1)} \tag{3.92}$$

$$\partial_{t_0} \sum_i \mathbf{v}_i F_i^{(0)} + \sum_i \mathbf{v}_i \mathbf{v}_i \cdot \nabla F_i^{(0)} = -\frac{1}{\tau_f} \sum_i F_i^{(1)}. \tag{3.93}$$

The RHS of each of these is zero because of the way we constructed the Chapman-Enskog expansion. We can also interchange the $\mathbf{v}_i$ and ∇ because $\mathbf{v}_i$ is a constant, getting:

$$\partial_{t_0} \sum_i F_i^{(0)} + \nabla \cdot \sum_i \mathbf{v}_i F_i^{(0)} = 0 \tag{3.94}$$

$$\partial_{t_0} \sum_i \mathbf{v}_i F_i^{(0)} + \nabla \cdot \sum_i \mathbf{v}_i \mathbf{v}_i F_i^{(0)} = 0 \quad (3.95)$$

or

$$\partial_{t_0} \sum_i F_i^{(0)} + \nabla \cdot (\sum_i \mathbf{v}_i F_i^{(0)}) = 0 \quad (3.96)$$

$$\partial_{t_0} (\rho \mathbf{u}) + \nabla \cdot \mathbf{\Pi}^{(0)} = 0 \quad (3.97)$$

with the definition

$$\mathbf{\Pi}^{(n)} \equiv \sum_i \mathbf{v}_i \mathbf{v}_i F_i^{(n)}. \quad (3.98)$$

Similarly for the magnetic field, consider the zeroth* moment of Eq.(3.90), which gives

$$\partial_{t_0} \sum_i G_{\alpha i}^{(0)} + \sum_i \mathbf{v}_i \cdot \nabla G_{\alpha i}^{(0)} = -\frac{1}{\tau_g} \sum_i G_{\alpha i}^{(1)} \quad (3.99)$$

which becomes

$$\partial_{t_0} \sum_i G_{\alpha i}^{(0)} + \nabla \cdot \sum_i \mathbf{v}_i G_{\alpha i}^{(0)} = 0 \quad (3.100)$$

or

$$\partial_{t_0} \sum_i G_{\alpha i}^{(0)} + \nabla \cdot \mathbf{\Lambda}^{(0)} = 0 \quad (3.101)$$

using the definition

$$\mathbf{\Lambda}^{(n)} \equiv \sum_i \mathbf{v}_i \mathbf{G}_i^{(n)}. \quad (3.102)$$

Thus, to lowest order in ϵ, the discrete Lattice Boltzmann method is solving the following equations:

$$\partial_{t_0} \sum_i F_i^{(0)} + \nabla \cdot (\sum_i \mathbf{v}_i F_i^{(0)}) = 0 \quad (3.103)$$

$$\partial_{t_0} (\sum_i \mathbf{v}_i F_i^{(0)}) + \nabla \cdot \mathbf{\Pi}^{(0)} = 0 \quad (3.104)$$

$$\partial_{t_0} \sum_i G_{\alpha i}^{(0)} + \nabla \cdot \mathbf{\Lambda}^{(0)} = 0. \quad (3.105)$$

*Only the zeroth moment of Eq.(3.90) is relevant for this analysis because **B** is only quantity whose physical behavior we are interested in reproducing.

If we go through a similar procedure on the Chapman-Enskog equation at the next higher power in ϵ, we find that

$$\partial_{t_1} \sum_i F_i^{(0)} = 0 \tag{3.106}$$

$$\partial_{t_1} (\sum_i \mathbf{v}_i F_i^{(0)}) + \nabla \cdot \left(1 - \frac{1}{2\tau_f}\right) \mathbf{\Pi}^{(1)} = 0 \tag{3.107}$$

$$\partial_{t_1} \sum_i G_{\alpha i}^{(0)} + \nabla \cdot \left(1 - \frac{1}{2\tau_g}\right) \mathbf{\Lambda}^{(1)} = 0. \tag{3.108}$$

Summing the first and second order moment equations, and neglecting higher order terms in ϵ, we get that:

$$\partial_t \sum_i F_i^{(0)} + \nabla \cdot (\sum_i \mathbf{v}_i F_i^{(0)}) = 0 \tag{3.109}$$

$$\partial_t (\sum_i \mathbf{v}_i F_i^{(0)}) + \nabla \cdot \left[\mathbf{\Pi}^{(0)} + \delta t \left(1 - \frac{1}{2\tau_f}\right) \mathbf{\Pi}^{(1)}\right] = O(\delta t^2) \tag{3.110}$$

$$\partial_t \sum_i G_{\alpha i}^{(0)} + \nabla \cdot \left[\mathbf{\Lambda}^{(0)} + \delta t \left(1 - \frac{1}{2\tau_g}\right) \mathbf{\Lambda}^{(1)}\right] = O(\delta t^2). \tag{3.111}$$

The goal then is to construct $F_i^{(0)}$ and $\mathbf{G}_i^{(0)}$ so that

$$\sum_i F_i^{(0)} = \rho \tag{3.112}$$

$$\sum_i \mathbf{v}_i F_i^{(0)} = \rho \mathbf{u} \tag{3.113}$$

$$\sum_i \mathbf{v}_i \mathbf{v}_i F_i^{(0)} \equiv \mathbf{\Pi}^{(0)} = \rho \mathbf{u}\mathbf{u} + \left(p + \frac{B^2}{2}\right) \mathbf{I} - \mathbf{B}\mathbf{B} \tag{3.114}$$

$$\sum_i \mathbf{v}_i \mathbf{G}_i^{(0)} \equiv \mathbf{\Lambda}^{(0)} = \mathbf{u}\mathbf{B} - \mathbf{B}\mathbf{u} \tag{3.115}$$

and the viscous and resistive effects are reproduced by the $\mathbf{\Pi}^{(1)}$ and $\mathbf{\Lambda}^{(1)}$ terms. We will find that we can successfully recover $\mathbf{\Pi}^{(0)}$ and $\mathbf{\Lambda}^{(0)}$, but that the $\mathbf{\Pi}^{(1)}$ and $\mathbf{\Lambda}^{(1)}$ terms will have some spurious components.

At this point we must introduce an ansatz for our solution if we are to continue. In order to introduce the ansatz, we need to also define our set of streaming vectors.

For the present work we will use the following, D3Q19, set of streaming vectors for the discretization of F

$$\mathbf{v}_i = v \times \begin{cases} (0,0,0) & i = 0 \\ (\pm 1,0,0),(0,\pm 1,0),(0,0,\pm 1) & i = 1,...,6 \\ (\pm 1,\pm 1,0),(\pm 1,0,\pm 1),(0,\pm 1,\pm 1) & i = 7,...,18 \end{cases} \tag{3.116}$$

and the D3Q7 set of streaming vectors for the discretization of $\mathbf{G}$

$$\mathbf{v}_i = v \times \begin{cases} (0,0,0) & i = 0 \\ (\pm 1,0,0),(0,\pm 1,0),(0,0,\pm 1) & i = 1,...,6\ . \end{cases} \tag{3.117}$$

These choices are motivated by the need for sufficient isotropy to ensure the possibility of satisfying Eqs.(3.114) and (3.115). Along with this velocity distribution, we must also propose an ansatz for the form of the $F^{(0)}$ and $\mathbf{G}^{(0)}$. For $F^{(0)}$ we propose the following ansatz:

$$F_i^{(0)} = \begin{cases} A_1 + B_1\mathbf{u}^2 + C_1\mathbf{B}^2 & i = 0 \\ A_2 + B_2\mathbf{u}^2 + C_2\mathbf{B}^2 + D_1(\mathbf{v}_i\cdot\mathbf{u}) + E_1(\mathbf{v}_i\cdot\mathbf{u})^2 + F_1(\mathbf{v}_i\cdot\mathbf{B})^2 & i = 1,...,6 \\ A_3 + B_3\mathbf{u}^2 + C_3\mathbf{B}^2 + D_2(\mathbf{v}_i\cdot\mathbf{u}) + E_2(\mathbf{v}_i\cdot\mathbf{u})^2 + F_2(\mathbf{v}_i\cdot\mathbf{B})^2 & i = 7,...,18\ . \end{cases} \tag{3.118}$$

As noted before, it is possible to arrive at an $F_i^{(0)}$ which satisfies Eq.(3.114), modulo the magnetic stress terms, and takes the form of the above ansatz by Taylor expanding the Maxwellian in $\mathbf{u}/c_s$ around $\mathbf{u} = 0$. While this *a priori* approach is somehow more satisfying the the ansatz approach, it does not always result in feasible numerical schemes. For example, consider [8] wherein the author demonstrates that when a LBM scheme for the shallow water equations is derived using such an *a priori* approach, the resulting numerical method is unstable. He shows that an alternate formulation for the equilibrium which is not the result of any *a priori* approach proves stable and accurate. This fact casts doubt on the general utility of *a priori* approaches. Furthermore, in the

case of $\mathbf{G}_i^{(0)}$, there is no obvious physical interpretation for $\mathbf{G}_i$. Thus, finding it in an *a priori* way seems unlikely.

Before continuing, it will prove helpful to introduce the following definitions of the rank-2 tensor $L^{(I)}_{\alpha\beta}$

$$L^{(I)}_{\alpha\beta} \equiv \sum_{i\in I} v_{i\alpha} v_{i\beta} \tag{3.119}$$

and the rank-4 tensor $L^{(I)}_{\alpha\beta\gamma\delta}$

$$L^{(I)}_{\alpha\beta\gamma\delta} \equiv \sum_{i\in I} v_{i\alpha} v_{i\beta} v_{i\gamma} v_{i\delta}. \tag{3.120}$$

In the case of the D3Q19 and D3Q7 streaming vectors, these tensors have the following values

$$L^{(I)}_{\alpha\beta} = v^2 \times \begin{cases} 0 & I = 0 \\ 2\delta_{\alpha\beta} & I = 1, ..., 6 \\ 8\delta_{\alpha\beta} & I = 7, ..., 18 \end{cases} \tag{3.121}$$

$$L^{(I)}_{\alpha\beta\gamma\delta} = v^4 \times \begin{cases} 0 & I = 0 \\ 2\delta_{\alpha\beta\gamma\delta} & I = 1, ..., 6 \\ 4(\Delta_{\alpha\beta\gamma\delta} - \delta_{\alpha\beta\gamma\delta}) & I = 7, ..., 18 \end{cases} \tag{3.122}$$

where the symbol $\Delta_{\alpha\beta\gamma\delta}$ is introduced as shorthand for $\delta_{\alpha\beta}\delta_{\gamma\delta} + \delta_{\alpha\gamma}\delta_{\beta\delta} + \delta_{\alpha\delta}\delta_{\beta\gamma}$. Also,

$$\delta_{\alpha\beta\gamma\delta} = \begin{cases} 1 & \text{if } \alpha = \beta = \gamma = \delta \\ 0 & \text{otherwise}\,. \end{cases} \tag{3.123}$$

We also note that all odd rank tensors, such as $\sum_{i\in I} v_{i\alpha} v_{i\beta} v_{i\gamma}$ will be 0, e.g.

$$L^{(I)}_{\alpha\beta\gamma} \equiv \sum_{i\in I} v_{i\alpha} v_{i\beta} v_{i\gamma} = v^3 \times \begin{cases} 0 & I = 0 \\ 0 & I = 1, ..., 6 \\ 0 & I = 7, ..., 18 \end{cases} \tag{3.124}$$

because of the lattice symmetries.

To continue, we must impose on our ansatz for $F_i^{(0)}$the following conditions:

$$\sum_{i=0}^{18} F_i^{(0)} = \rho \tag{3.125}$$

$$\sum_{i=0}^{18} \mathbf{v}_i F_i^{(0)} = \rho\mathbf{u} \tag{3.126}$$

$$\sum_{i=0}^{18} \mathbf{v}_i\mathbf{v}_i F_i^{(0)} \equiv \mathbf{\Pi}^{(0)} = \rho\mathbf{u}\mathbf{u} + \left(p + \frac{B^2}{2}\right)\mathbf{I} - \mathbf{B}\mathbf{B}. \tag{3.127}$$

Using our ansatz for $F_i^{(0)}$ and the tensor definitions given above, the first requirement, Eq.(3.125), can simplified as follows

$$\begin{aligned}
\sum_{i=0}^{18} F_i^{(0)} = & \quad (A_1 + 6A_2 + 12A_3) \\
& + (C_1 + 6C_2 + 12C_3)\cdot\mathbf{B}^2 + (B_1 + 6B_2 + 12B_3)\cdot\mathbf{u}^2 \\
& + (E_1 u_\alpha u_\beta + F_1 B_\alpha B_\beta)\cdot L_{\alpha\beta}^{(1-6)} + (E_2 u_\alpha u_\beta + F_2 B_\alpha B_\beta)\cdot L_{\alpha\beta}^{(7-18)} \\
= & \quad (A_1 + 6A_2 + 12A_3) \\
& + (C_1 + 6C_2 + 12C_3)\cdot\mathbf{B}^2 + (B_1 + 6B_2 + 12B_3)\cdot\mathbf{u}^2 \\
& + (E_1 u_\alpha u_\beta + F_1 B_\alpha B_\beta)\cdot 2v^2\delta_{\alpha\beta} + (E_2 u_\alpha u_\beta + F_2 B_\alpha B_\beta)\cdot 8v^2\delta_{\alpha\beta} \\
= & \quad (A_1 + 6A_2 + 12A_3) \\
& + (C_1 + 6C_2 + 12C_3)\cdot\mathbf{B}^2 + (B_1 + 6B_2 + 12B_3)\cdot\mathbf{u}^2 \\
& + (E_1\mathbf{u}^2 + F_1\mathbf{B}^2)\cdot 2v^2 + (E_2\mathbf{u}^2 + F_2\mathbf{B}^2)\cdot 8v^2
\end{aligned} \tag{3.128}$$

Collecting the coefficients of $\mathbf{u}^2$ and $\mathbf{B}^2$ we get:

$$\begin{aligned}
\sum_{i=0}^{18} F_i^{(0)} = & \quad (A_1 + 6A_2 + 12A_3) \\
& + (B_1 + 6B_2 + 12B_3 + 2v^2E_1 + 8v^2E_2)\cdot\mathbf{u}^2 \\
& + (C_1 + 6C_2 + 12C_3 + 2v^2F_1 + 8v^2F_2)\cdot\mathbf{B}^2.
\end{aligned} \tag{3.129}$$

Now, comparing this with the constraint in Eq.(3.125), it is evident that we need

$$\begin{aligned} A_1 + 6A_2 + 12A_3 &= \rho && (3.130)\\ B_1 + 6B_2 + 12B_3 + 2v^2E_1 + 8v^2E_2 &= 0 && (3.131)\\ C_1 + 6C_2 + 12C_3 + 2v^2F_1 + 8v^2F_2 &= 0 && (3.132) \end{aligned}$$

in order for this constraint to hold. Similarly, for Eq.(3.126) we get that

$$\begin{aligned} \sum_{i=0}^{18} \mathbf{v}_i F_i^{(0)} &= D_1 u_\beta L_{\alpha\beta}^{(1-6)} + D_2 u_\beta L_{\alpha\beta}^{(7-18)} \\ &= 2D_1 u_\beta \delta_{\alpha\beta} v^2 + 8D_2 u_\beta \delta_{\alpha\beta} v^2 \\ &= v^2(2D_1 + 8D_2) u_\alpha && (3.133) \end{aligned}$$

Evidently, in order for Eq.(3.126) to hold, we need that

$$2D_1 v^2 + 8D_2 v^2 = \rho. \qquad (3.134)$$

Finally, for the constraint in Eq.(3.127) we get that

$$\begin{aligned} \sum_{i=0}^{18} \mathbf{v}_i \mathbf{v}_i F_i^{(0)} = & \quad (2v^2A_2 + 8v^2A_3) \cdot \delta_{\alpha\beta} \\ & + (2v^2B_2 + 8v^2A_3) \cdot \mathbf{u}^2 \delta_{\alpha\beta} + (2v^2C_2 + 8v^2C_3) \cdot \mathbf{B}^2 \delta_{\alpha\beta} \\ & + (v^4E_1 u_\gamma u_\delta + v^4F_1 B_\gamma B_\delta) \cdot 2\delta_{\alpha\beta\gamma\delta} \\ & + (v^4E_2 u_\gamma u_\delta + v^4F_2 B_\gamma B_\delta) \cdot 4(\Delta_{\alpha\beta\gamma\delta} - \delta_{\alpha\beta\gamma\delta}) \\ = & \quad (2v^2A_2 + 8v^2A_3) \cdot \delta_{\alpha\beta} + \\ & + (2v^2B_2 + 8v^2B_3 + 4v^4E_2) \cdot \mathbf{u}^2 \delta_{\alpha\beta} + (2v^2C_2 + 8v^2C_3 + 4v^4F_2) \cdot \mathbf{B}^2 \delta_{\alpha\beta} \\ & + \Big[(2v^4E_1 - 4v^4E_2) u_\alpha u_\beta + (2v^4F_1 - 4v^4F_2) B_\alpha B_\beta \Big] \cdot \delta_{\alpha\beta} \\ & + 8v^4E_2 u_\alpha u_\beta + 8v^4F_2 B_\alpha B_\beta \,. \qquad (3.135) \end{aligned}$$

Thus, in order for Eq.(3.127) to hold, we need the following relationships among the

coefficients:

$$
\begin{aligned}
2v^2A_2 + 8v^2A_3 &= c_s^2\rho && (3.136)\\
2v^2B_2 + 8v^2B_3 + 4v^4E_2 &= 0 && (3.137)\\
2v^2C_2 + 8v^2C_3 + 4v^4F_2 &= \frac{1}{2} && (3.138)\\
2v^4E_1 - 4v^4E_2 &= 0 && (3.139)\\
2v^4F_1 - 4v^4F_2 &= 0 && (3.140)\\
8v^4E_2 &= \rho && (3.141)\\
8v^4F_2 &= -1. && (3.142)
\end{aligned}
$$

Thus far, we have found the constraints on the coefficients necessary for satisfying Eqs.(3.125), (3.126), and (3.127); however, the set of constraints still does not uniquely determine the coefficients. To continue, we now examine the $\mathbf{\Pi}^{(1)}$ that results from our ansatz:

$$
\mathbf{\Pi}^{(1)} = \sum_{i=0}^{18} \mathbf{v}_i\mathbf{v}_i F_i^{(1)} \tag{3.143}
$$

which, using Eq.(3.90) can be written as

$$
\begin{aligned}
\mathbf{\Pi}^{(1)} = \Pi_{\alpha\beta}^{(1)} &= \sum_{i=0}^{18} \mathbf{v}_i\mathbf{v}_i \left[-\tau_f(\partial_{t_0} + \mathbf{v}_i\cdot\nabla)F_i^{(0)}\right]\\
&= -\tau_f\left[\partial_{t_0}\sum_{i=0}^{18}\mathbf{v}_i\mathbf{v}_i F_i^{(0)} - \nabla\cdot\sum_{i=0}^{18}\mathbf{v}_i\mathbf{v}_i\mathbf{v}_i F_i^{(0)}\right]\\
&= -\tau_f\left[\partial_{t_0}\Pi_{\alpha\beta}^{(0)} + \partial_\gamma\left(D_1u_\delta L_{\alpha\beta\gamma\delta}^{(1-6)} + D_2u_\delta L_{\alpha\beta\gamma\delta}^{(7-18)}\right)\right]
\end{aligned}
$$

which can be written, substituting the expression for $\Pi_{\alpha\beta}^{(0)}$, and making a few simplifications

$$
\begin{aligned}
-\frac{1}{\tau_f}\Pi_{\alpha\beta}^{(1)} = \quad & \partial_{t_0}\left[\left(c_s^2\rho + \frac{1}{2}B_\gamma B_\gamma\right)\delta_{\alpha\beta} + \rho u_\alpha u_\beta - B_\alpha B_\beta\right]\\
+ \quad & \partial_\gamma(4v^4D_2u_\gamma)\delta_{\alpha\beta} + \partial_\alpha(4v^4D_2u_\beta) + \partial_\beta(4v^4D_2u_\alpha)\\
- \quad & \partial_\alpha(2v^4D_1 - 4v^4D_2)u_\beta\delta_{\alpha\beta}. \qquad (3.144)
\end{aligned}
$$

For isotropy, we need the last term to be zero:

$$\partial_\alpha(2v^2D_1 - 4v^2D_2)u_\beta\delta_{\alpha\beta} = 0 \quad \Rightarrow \quad 2v^2D_1 - 4v^2D_2 = 0 \tag{3.145}$$

which, recalling Eq.(3.134), results in $D_1 = \frac{\rho}{6v^2}$ and $D_2 = \frac{\rho}{12v^2}$. Using this, $\Pi^{(1)}_{\alpha\beta}$ may be written, after some substitutions, as

$$\begin{aligned} -\frac{1}{\tau_f}\Pi^{(1)}_{\alpha\beta} = & \quad B_\gamma\partial_\eta\Lambda_{\gamma\eta}\delta_{\alpha\beta} + B_\alpha\partial_\eta\Lambda_{\beta\eta} + B_\beta\partial_\eta\Lambda_{\alpha\eta} \\ & + \left(\frac{v^2}{3} - c_s^2\right)\partial_\gamma(\rho u_\gamma)\delta_{\alpha\beta} + \frac{v^2}{3}\partial_\alpha(\rho u_\beta) + \frac{v^2}{3}\partial_\beta(\rho u_\alpha) \\ & - u_\beta\partial_\alpha(c_s^2\rho) - u_\alpha\partial_\beta(c_s^2\rho) - \partial_\gamma(\rho u_\alpha u_\beta u_\gamma) \end{aligned} \tag{3.146}$$

which can be further rearranged to

$$\begin{aligned} -\frac{1}{\tau_f}\Pi^{(1)}_{\alpha\beta} = & \quad B_\gamma\partial_\eta\Lambda_{\gamma\eta}\delta_{\alpha\beta} + B_\alpha\partial_\eta\Lambda_{\beta\eta} + B_\beta\partial_\eta\Lambda_{\alpha\eta} \\ & + \frac{v^2}{3}\rho(\partial_\alpha u_\beta + \partial_\beta u_\alpha) - \partial_\gamma(\rho u_\alpha u_\beta u_\gamma) \\ & + \left(\frac{v^2}{3} - c_s^2\right)\partial_\gamma(\rho u_\gamma)\delta_{\alpha\beta} + \left(\frac{v^2}{3} - c_s^2\right)(u_\alpha\partial_\beta\rho + u_\beta\partial_\alpha\rho). \end{aligned} \tag{3.147}$$

Looking at Eq.(3.147) we can see that the third term is the only term which we want to be present if we are to recover a sensible strain tensor $\mathbf{S}$. The presence of the other extraneous terms must be dealt with. Clearly, if we take $c_s^2 = \frac{v^2}{3}$ then we will eliminate the last two terms. This gives another restriction on the A coefficients in our ansatz. The first, second, third, and fifth terms cannot be so conveniently eliminated. If, however, we imagine rescaling u by the sound speed c_s, then $\partial_\gamma(\rho u_\alpha u_\beta u_\gamma)$ is $O(\mathrm{Ma}^3)$. As we discussed previously, this term can be neglected for small mach number.

To address the first three terms, we note that they each contain a piece that of the form $B_\gamma\partial_\eta(u_\alpha B_\eta - B_\alpha u_\eta)$. Now, rescaling u by the sound speed c_s, and B by $c_s\sqrt{\rho}$, these terms are seen to be $O(\mathrm{Ma}\beta^{-1})$ were we have used that $\beta = c_s^2/c_a^2$ and $c_a \equiv B/\sqrt{\rho}$.

Thus, as Ma $\to 0$ and $\beta \to \infty$, these equations are consistent with the standard MHD equations because the suprious terms go to zero faster than the physical terms in the MHD equations. The scheme may therefore be said to be consistent with the MHD equations in the high-β, low Mach number regime.*

So far, we have found 12 equations relating the coefficients of our ansatz; however, we have 16 unknowns if we count the sound speed c_s as an unknown.* We need four more equations in order to uniquely determine the system. Consider the following four equations:

$$\frac{A_1}{A_2} = \frac{B_1}{B_2} = \frac{C_1}{C_2} = 3\frac{A_2}{A_3} = 3\frac{B_2}{B_3} = \chi. \tag{3.148}$$

In the D2Q9 hydrodynamic case, imposing the analogous relations results in the standard D2Q9 equilibrium distribution discussed in the introduction [29]. Imposing these restrictions here, the resultant equilibrium can be written:

$$F_i^{(0)} = \begin{cases} \frac{12}{12}\rho\left[\frac{1}{3} - \frac{1}{2v^2}\mathbf{u}^2\right] & i = 0 \\ \frac{2}{12}\rho\left[\frac{1}{3} - \frac{1}{2v^2}\mathbf{u}^2 + \frac{1}{v^2}(\mathbf{v}_i\cdot\mathbf{u}) + \frac{3}{v^4}(\mathbf{v}_i\cdot\mathbf{u})^2 - \frac{3}{2v^4}(\mathbf{v}_i\cdot\mathbf{B})^2\right] & i = 1,...,6 \\ \frac{1}{12}\rho\left[\frac{1}{3} - \frac{1}{2v^2}\mathbf{u}^2 + \frac{1}{v^2}(\mathbf{v}_i\cdot\mathbf{u}) + \frac{3}{v^4}(\mathbf{v}_i\cdot\mathbf{u})^2 - \frac{3}{2v^4}(\mathbf{v}_i\cdot\mathbf{B})^2 + \frac{3}{2v^2}\mathbf{B}^2\right] & i = 7,...,18 \end{cases}$$

where $\chi = 2$ and $c_s^2 = \frac{v^2}{3}$. Interestingly, the sound speed that results from these extra, arbitrary, equations is precisely the one that cancels some of the extraneous terms in $\mathbf{\Pi}^{(1)}$. Going back to Eq.(3.110), we see that, in the Ma $\to 0$ and $\beta \to \infty$ limit, $\rho\mathbf{u}$ is evolving according to

$$\partial_t(\rho\mathbf{u}) + \nabla\cdot\left[\mathbf{\Pi} - \delta t\tau_f\left(1 - \frac{1}{2\tau_f}\right)\frac{2v^2}{3}\rho\mathbf{S}\right] = 0 \tag{3.149}$$

*The β of a plasma is defined as the ratio of the hydrodynamic pressure $c_s\rho$ to the magnetic pressure $B^2/2$.

*We could regard c_s as an adjustable parameter; however, this results in very ugly solution for the coefficients. It is convenient to exchange the free parameter c_s for the free parameter χ defined in Eq.(3.148).

which is consistent with the MHD equations if we take

$$\nu = \delta t \left(\tau_f - \frac{1}{2}\right) \frac{v^2}{3}. \tag{3.150}$$

We turn our attention now to deriving an appropriate $\mathbf{G}_i$. We use the following ansatz

$$\mathbf{G}_i^{(0)} = \begin{cases} M_1 \mathbf{B}^2 & i = 0 \\ M_2 \mathbf{B}^2 + N_1 \mathbf{B}(\mathbf{v}_i \cdot \mathbf{u}) + N_2 \mathbf{u}(\mathbf{v}_i \cdot \mathbf{B}) & i = 1, ..., 6 \end{cases} \tag{3.151}$$

which is the simplest form capable of satisfying Eq.(3.115) [9]. In analogy with $F_i^{(0)}$, the constraints that this equilibrium must satisfy to recover the MHD equations at lowest order in the Chapman-Enskog expansion are

$$\sum_{i=0}^{6} \mathbf{G}_i^{(0)} = \mathbf{B} \tag{3.152}$$

$$\sum_{i=0}^{6} \mathbf{v}_i \mathbf{G}_i^{(0)} \equiv \mathbf{\Lambda}^{(0)} = \mathbf{uB} - \mathbf{Bu}. \tag{3.153}$$

The first of these constraints implies

$$\sum_{i=0}^{6} \mathbf{G}_i^{(0)} = (M_1 + 6M_2)\mathbf{B} = \mathbf{B} \quad \Rightarrow \quad M_1 + 6M_2 = 1. \tag{3.154}$$

The second constraint,

$$\sum_{i=0}^{6} \mathbf{v}_i \mathbf{G}_i^{(0)} = 2v^2 \left[N_1 \mathbf{uB} + N_2 \mathbf{Bu}\right] = \mathbf{uB} - \mathbf{Bu}, \tag{3.155}$$

implies that

$$N_1 = \frac{1}{2v^2} \tag{3.156}$$

$$N_2 = -\frac{1}{2v^2}. \tag{3.157}$$

Evidently, we still have some freedom in our choice for M_1 and M_2. We make the choice which results in

$$\mathbf{G}_i^{(0)} = \begin{cases} \frac{1}{4}\mathbf{B}^2 & i = 0 \\ \frac{1}{8}\mathbf{B}^2 + \frac{1}{2v^2}\left[\mathbf{B}(\mathbf{v}_i \cdot \mathbf{u}) - \mathbf{u}(\mathbf{v}_i \cdot \mathbf{B})\right] & i = 1, ..., 6\,. \end{cases} \tag{3.158}$$

We acknowledge that this choice is arbitrary. In [16], the author retains this flexibility as an additional parameter for adjusting the resistivity. Futher work should be done to determine the significance of this free parameter, if any. Examining $\mathbf{\Lambda}^{(2)}$, for instance, might reveal a rationale for setting M_1 and M_2. To recover the dissipative behavior for $\mathbf{B}$, we can derive $\mathbf{\Lambda}^{(1)}$ in the same way we derived $\mathbf{\Pi}^{(1)}$:

$$\begin{aligned} \mathbf{\Lambda}^{(1)} &= \sum_{i=0}^{6} \mathbf{v}_i \mathbf{G}_i^{(1)} \\ &= \sum_{i=0}^{6} \mathbf{v}_i \left[-\tau_g(\partial_{t_0} + \mathbf{v}_i \cdot \nabla)\mathbf{G}_i^{(0)}\right] \\ &= -\tau_g \left[\partial_{t_0} \sum_{i=0}^{6} \mathbf{v}_i \mathbf{G}_i^{(0)} + \nabla \cdot \sum_{i=0}^{6} \mathbf{v}_i \mathbf{v}_i \mathbf{G}_i^{(0)}\right] \\ &= -\tau_g \left[\partial_{t_0} \mathbf{\Lambda}_0 + \frac{v^2}{4}\nabla \mathbf{B}\right] \end{aligned} \tag{3.159}$$

Expanding $\partial_{t_0}\mathbf{\Lambda}_0$, one finds a series of $O(\beta^{-\frac{3}{2}})$, $O(\mathrm{Ma}\beta^{-1})$, and $O(\mathrm{Ma}^2\beta^{-\frac{1}{2}})$ terms. We can thus write $\mathbf{\Lambda}^{(1)}$ as

$$\mathbf{\Lambda}^{(1)} = -\tau_g \frac{v^2}{4}\nabla \mathbf{B} + O(\beta^{-\frac{3}{2}}) + O(\mathrm{Ma}\beta^{-1}) + O(\mathrm{Ma}^2\beta^{-\frac{1}{2}}). \tag{3.160}$$

Going back to Eq.(3.111), we see that, neglecting the small extraneous terms in $\mathbf{\Lambda}^{(1)}$ by assuming high-β and low Mach number, $\mathbf{B}$ is evolving according to

$$\partial_t \mathbf{B} + \nabla \cdot \left[\mathbf{\Lambda}^{(0)} - \delta t \tau_g \left(1 - \frac{1}{2\tau_g}\right) \frac{v^2}{4}\nabla \mathbf{B}\right] = 0 \tag{3.161}$$

which is consistent with the MHD induction equation if we take

$$\eta = \delta t \left(\tau_g - \frac{1}{2}\right) \frac{v^2}{4}. \tag{3.162}$$

Chapter 4
Multi-Block Refinement Scheme

One way of improving the performance of numerical schemes involving discrete grids is to concentrate grid points—and thus computational effort—in areas of localized small scale structure. Recently there has been work on developing schemes that allow such refinement in the context of lattice Boltzmann methods [21] [12] [11] [16]. The most well-known scheme, described in [12], outlines a "multi-block" strategy for spatial domain decomposition in LBMs. In this method, one divides the spatial domain into a set of blocks B_i, each of which can have a different spatial resolution δx_i. One restriction with this method is that grid cells in a block have dimensions that are integer multiples of the grid cell dimensions in all neighboring blocks.

The blocks in this scheme propagate the density functions F_i across their interfaces during the streaming step of the LBM algorithm. In order for the values of the field variables and stress tensors to be consistent on the different blocks, we must transform the densities F_i appropriately. Also, in order to ensure that the physical values of the viscosity ν and resistivity η are constant across the entire domain, we must tune the relaxation parameter τ in each block. We discuss the consequences of these requirements and the resulting scheme below.

4.1 Maintaining ν and η

If we have a computational domain which has been subdivided into blocks, we would generally like to ensure that the physical value of the viscosity and resistivity is the same for each block. Consider two blocks: one has a coarse spacing δx_c, and one has a fine spacing δx_f. Recall that the Chapman-Enskog expansion shows that the physical value of the viscosity ν can be written as a function of the dimensionless relaxation parameter

τ and the time step δt. Indeed, for a general LBM method, ν will take the form

$$\nu = \alpha(\tau - \frac{1}{2})\delta t = \alpha(\tau - \frac{1}{2})\frac{\delta x}{v} \tag{4.1}$$

where α is a constant related to the lattice structure. The value of the viscosity in each of our blocks is then

$$\nu_c = \frac{\alpha}{v}(\tau_c - \frac{1}{2})\delta x_c \tag{4.2}$$

$$\nu_f = \frac{\alpha}{v}(\tau_f - \frac{1}{2})\delta x_f \tag{4.3}$$

assuming the blocks use the same set of streaming vectors. Now, if these two blocks are each part of some larger simulation domain, we would generally want $\nu_c = \nu_f$, which implies that, using Eqs.(4.2) and (4.3),

$$\tau_f = \frac{\delta x_c}{\delta x_f}\left(\tau_c - \frac{1}{2}\right) + \frac{1}{2}. \tag{4.4}$$

A similar line of reasoning results in the same condition for preserving constant resistivity η. Thus, if the relaxation parameters for F and $\mathbf{G}$ both sastify Eq.(4.4), then $\nu_c = \nu_f$ and $\eta_c = \eta_f$.

4.2 Block Interface Propagation

The other condition that we would like to enforce involves the propagation of information between grids. Consider again two grids, one with a coarse spacing δx_c and one with a fine spacing δx_f. We will denote the density functions on these grids as $F_i^{(c)}$ and $F_i^{(f)}$, respectively. Consider spliting $F_i^{(c)}$ and $F_i^{(f)}$ into their equilibrium and non-equilibrium parts:

$$F_i^{(c)} = F_i^{(c,0)} + \left[\sum_{n=1}^{\infty} \epsilon^n F_i^{(c,n)}\right] = F_i^{(c,0)} + [F_i^{(c,neq)}] \tag{4.5}$$

$$F_i^{(f)} = F_i^{(f,0)} + \left[\sum_{n=1}^{\infty} \epsilon^n F_i^{(f,n)}\right] = F_i^{(f,0)} + [F_i^{(f,neq)}]. \tag{4.6}$$

Using the lattice BGK equation, one can show that, denoting $F_i(\mathbf{x}, t+\delta t)$ as $\tilde{F}_i$ the following transformations are necessary to preserve the continuity of the stress tensors and field variables across the interface:

$$\tilde{F}_i^{(c)} = F_i^{(f,0)} + m\frac{\tau_c - 1}{\tau_f - 1}\left[\tilde{F}_i^{(f)} - F_i^{(f,0)}\right] \tag{4.7}$$

$$\tilde{F}_i^{(f)} = F_i^{(c,0)} + \frac{1}{m}\frac{\tau_f - 1}{\tau_c - 1}\left[\tilde{F}_i^{(c)} - F_i^{(c,0)}\right] \tag{4.8}$$

where $m \equiv \delta x_c / \delta x_f$ [12]. These are the equations we will use to transform densities at the block interfaces. More recently, some authors have proposed other ways of transforming the density function F at the interface [11]. For a detailed description of how the algorithm proceeds, we refer the reader to [21]. Here we give a brief description to bring up a few key points.

Imagine dividing the plane along a straight line into two blocks, one block with cells twice the width of the other block. These two blocks will overlap by a single coarse cell width. At $t = 0$, the coarse grid is advanced a single time step to reach $t = 1.0$. Next, the fine grid will be advanced by two time steps. The first brings it to $t = 0.5$, and the second brings it to $t = 1.0$. We need two steps since $\delta x = v\delta t$: halving the cell size implies halving the time step. Now, for the first time step, the fine grid does not need any information from the coarse grid because it has the necessary boundary conditions from the initial conditions; however, for the second time step from $t = 0.5$ to $t = 1.0$, the values of the incoming distribution functions will need to be supplied from the coarse grid. To do this we must interpolate between the coarse grid solution at $t = 0$ and $t = 1$. Not only must we interpolate temporally, we must interpolate spatially to recover the values of the intermediate fine grid points. In the spirit of preserving the spatial locality of the scheme, we choose to interpolate linearly in space. In [12], the authors use a cubic spline for the spatial interpolation. Using a cubic spline for the interpolation negates the locality of the lattice Boltzmann scheme, and we thus choose to avoid it. In time we

interpolate linearly for the first time step and quadratically thereafter using what would in this case would be $t = -1$, $t = 0$ and $t = 1$.

Chapter 5
Validation

In this chapter we present a series of numerical tests. The purpose of these will be to verify some basic features of the lattice kinetic scheme we have developed. To test the multi-block refinement scheme, we also present a comparison between what we will call the *single-block* and *dual-block* cases. The single-block case is merely the lattice kinetic scheme we have derived earlier without multi-block refinement. In the dual-block case we have divided the domain into two equal sized blocks along the line $x = 0.5$. On one half, we have refined the grids cell to be half the width of the cells on the other side of the interface. We use the scheme described in the last chapter to propagate the distribution functions across the boundary. For all tests, we use a periodic box. All simulations are done on an Intel architecture in double precision. The code is written in Fortran90.

First we test for the proper reproduction of the linear MHD magnetosonic and shear Alfven modes. In the case of the Alfven waves, we verify that both the real and imaginary parts of the dispersion relation are correctly reproduced. We also verify the second order convergence in δx—or equivalently δt—for the Alfven waves. We then proceed to the non-linear Orszag-Tang problem [18]. For this problem, we will focus our attention on the scheme's convergence properties in the single-block and dual-blocks cases. We also examine the preservation of $\nabla \cdot \mathbf{B}$ and verify conservation of mass.

Before proceeding to these tests, we present a derivation of the linear MHD eigenmodes. Such a derivation can be found in many texts, e.g. [26]. We favor the derivation in [22] as unusually transparent and use it as the motivation for what is presented here.

5.1 MHD Eigenmodes

We present here a derivation of the linear MHD eigenmodes which we will then verify the code reproduces. We begin with the standard ideal MHD equations derived

previously:

$$\partial_t \rho + \nabla \cdot (\rho \mathbf{u}) = 0 \tag{5.1}$$

$$\partial_t (\rho \mathbf{u}) + \nabla (\rho \mathbf{u}\mathbf{u}) + \nabla p - (\nabla \times \mathbf{B}) \times \mathbf{B} = 0 \tag{5.2}$$

$$\partial_t \mathbf{B} - \nabla \times (\mathbf{u} \times \mathbf{B}) = 0. \tag{5.3}$$

We begin by looking for solutions which are small perturbations to some background density ρ_0 and magnetic field $\mathbf{B}_0$. To do this, we make the following substitutions:

$$\rho = \rho_0 + \tilde{\rho} \tag{5.4}$$

$$\mathbf{B} = \mathbf{B}_0 + \tilde{\mathbf{B}} \tag{5.5}$$

$$\mathbf{u} = \mathbf{0} + \tilde{\mathbf{u}} \tag{5.6}$$

where we take $\tilde{\mathbf{B}} \ll \mathbf{B}_0$ and $\tilde{\rho} \ll \rho_0$. Making these substitutions and dropping terms that are the product of two or more small quantities, we get the following linearized set of ideal MHD equations:

$$\partial_t \tilde{\rho} + \rho_0 \nabla \cdot \tilde{\mathbf{u}} = 0 \tag{5.7}$$

$$\rho_0 \partial_t \tilde{\mathbf{u}} + c_s^2 \nabla \tilde{\rho} - (\nabla \times \tilde{\mathbf{B}}) \times \mathbf{B}_0 = 0 \tag{5.8}$$

$$\partial_t \tilde{\mathbf{B}} - \nabla \times (\tilde{\mathbf{u}} \times \mathbf{B}_0) = 0 \tag{5.9}$$

where we have used the iso-thermal closure discussed earlier. To find the wave-like solutions, we assume the perturbations take the following form:

$$\tilde{\rho} = \tilde{\rho} e^{i(\mathbf{k}\cdot\mathbf{x} - \omega t)} \tag{5.10}$$

$$\tilde{\mathbf{B}} = \tilde{\mathbf{B}} e^{i(\mathbf{k}\cdot\mathbf{x} - \omega t)} \tag{5.11}$$

$$\tilde{\mathbf{u}} = \tilde{\mathbf{u}} e^{i(\mathbf{k}\cdot\mathbf{x} - \omega t)}. \tag{5.12}$$

Making these substitutions into the linearized equations, we get the following:

$$\omega\tilde{\rho} - \rho_0(\mathbf{k}\cdot\tilde{\mathbf{u}}) = 0 \tag{5.13}$$

$$\omega\rho_0\tilde{\mathbf{u}} - c_s^2\mathbf{k}\tilde{\rho} + (\mathbf{k}\times\tilde{\mathbf{B}})\times\mathbf{B}_0 = 0 \tag{5.14}$$

$$\omega\tilde{\mathbf{B}} + \mathbf{k}\times(\tilde{\mathbf{u}}\times\mathbf{B}_0) = 0. \tag{5.15}$$

If we eliminate $\tilde{\mathbf{B}}$ and $\tilde{\rho}$ from this system, the result is:

$$\left[\omega^2 - \frac{(\mathbf{k}\cdot\mathbf{B}_0)^2}{\rho_0}\right]\tilde{\mathbf{u}} - \left[\left(c_s^2 + \frac{\mathbf{B}_0^2}{\rho_0}\right)\mathbf{k} - \frac{\mathbf{k}\cdot\mathbf{B}_0}{\rho_0}\mathbf{B}_0\right](\mathbf{k}\cdot\tilde{\mathbf{u}}) + \frac{(\tilde{\mathbf{u}}\cdot\mathbf{B}_0)(\mathbf{k}\cdot\mathbf{B}_0)}{\rho_0}\mathbf{k} = 0. \tag{5.16}$$

This can be written as

$$\mathbf{A}\tilde{\mathbf{u}} = \mathbf{0} \tag{5.17}$$

with

$$\mathbf{A} = \begin{pmatrix} \omega^2 - k^2c_A^2 - k^2c_s^2\sin^2\theta & 0 & -k^2c_s^2\sin\theta\cos\theta \\ 0 & \omega^2 - k^2c_a^2\cos^2\theta & 0 \\ -k^2c_s^2\sin\theta\cos\theta & 0 & \omega^2 - k^2c_s^2\sin^2\theta \end{pmatrix} \tag{5.18}$$

by taking $\mathbf{B}_0 = B_0\hat{\mathbf{z}}$ and $k_y = 0$ (i.e., that $\mathbf{k}$ lies in the x, z plane). We use θ as the angle between $\mathbf{B}_0$ and $\mathbf{k}$, and define the Alfven speed $c_a^2 \equiv \frac{B_0^2}{\rho_0}$. These assumptions only serve to define the coordinates of any physical problem, they do not restrict the class of solutions supported by Eq.(5.16).

We find solutions to Eq.(5.17) by setting $\det\mathbf{A} = 0$ and solving the resulting characteristic equation for ω. This results in the following solutions for ω:

$$\omega = kc_a \quad \text{(alfven wave)} \tag{5.19}$$

$$\omega = kc_{m_f} \quad \text{(fast magnetosonic wave)} \tag{5.20}$$

$$\omega = kc_{m_s} \quad \text{(slow magnetosonic wave).} \tag{5.21}$$

where

$$c_{m_f}^2 = \frac{1}{2}\left[c_a^2 + c_s^2 + \sqrt{c_a^4 + c_s^4 - 2c_a^2 c_s^2 \cos 2\theta}\right] \tag{5.22}$$

$$c_{m_s}^2 = \frac{1}{2}\left[c_a^2 + c_s^2 - \sqrt{c_a^4 + c_s^4 - 2c_a^2 c_s^2 \cos 2\theta}\right]. \tag{5.23}$$

The un-normalized eigenvectors $\tilde{\mathbf{u}}$ corresponding to these waves are

$$\tilde{\mathbf{u}}_a = \begin{pmatrix} 0 \\ 1 \\ 0 \end{pmatrix} \tag{5.24}$$

$$\tilde{\mathbf{u}}_{m_f} = \begin{pmatrix} \frac{c_a^2 - c_s^2\cos 2\theta + \sqrt{c_a^4 + c_s^4 - 2c_a^2c_s^2\cos 2\theta}}{c_s^2 \sin 2\theta} \\ 0 \\ 1 \end{pmatrix} \tag{5.25}$$

$$\tilde{\mathbf{u}}_{m_s} = \begin{pmatrix} \frac{c_a^2 - c_s^2\cos 2\theta - \sqrt{c_a^4 + c_s^4 - 2c_a^2c_s^2\cos 2\theta}}{c_s^2 \sin 2\theta} \\ 0 \\ 1 \end{pmatrix}. \tag{5.26}$$

We can compute the corresponding perturbations to $\mathbf{B_0}$ and ρ_0 by going back to Eqs.(5.13) and Eq.(5.15).

5.2 Alfven Dispersion

In this section we examine the evolution of Alfven waves in the code. First, we test that the real part of the dispersion relation $\omega = c_a k$ is properly reproduced by the code. To test this, we setup the Alfven velocity and magnetic perturbations for a traveling—as opposed to standing—Alfven wave. We begin by setting $\mathbf{k} \parallel \mathbf{B}$ and aligning both with the grid so that

$$\mathbf{B} = (B_x, B_y, B_z) = (B_0, 0, \tilde{B}_z \cos(2\pi x)) \tag{5.27}$$

where we use $\tilde{B}_z/B_0 = 1000$. We then recover the effective ω of the code using a least squares fit to the code output, as shown in Fig. 5.1. We vary the magnitude of $\mathbf{k}$ and

plot the results in Fig. 5.2.* Fig. 5.3 shows the relative error in the wave period. The grid-scale Alfven wave shows a relative error in period of about 15 percent. At 16 grid points per wavelength, this error is about one part in 1000. As Fig. 5.3 shows, this relative error decreases as the square of the number of grid points per wavelength. This suggests that the real part of the Alfven dispersion is being properly reproduced by the numerical scheme.

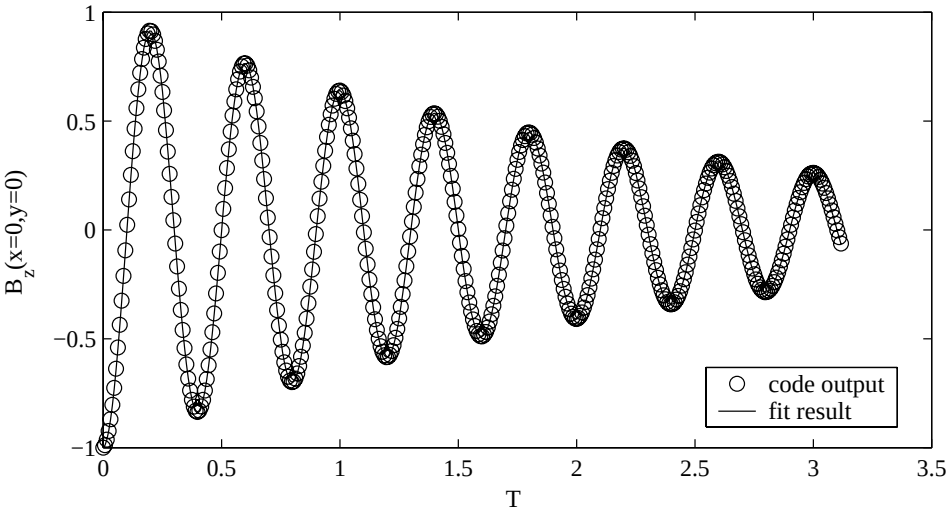

Figure 5.1 A normalized B_z at $(x, y) = (0, 0)$ as a function of time in one of the test cases. A least-squares fit to this curve recovers the real and imaginary components of the dispersion produced by the code. This fit is typical, showing good agreement with the code output.

For the dual-block case, we present figures showing the propagation of this Alfven wave across the block interface. For this case, we set very low resistivity and viscosity, $\eta = \nu = 10^{-6}$. Fig. 5.4 shows the case when $\lambda = 4$ coarse grid cells. Although the case with $\lambda = 4$ shows that the wave has become deformed after one period of propagation, the case for $\lambda = 8$ in Fig. 5.5 and $\lambda = 16$ in Fig. 5.6 show almost no deformation. Furthermore, the stability of the code for this linear problem even with very small η and

*We use the wave period $T = \frac{2\pi}{\omega}$ and $\lambda = \frac{2\pi}{k}$ as the plotting variables because their units are more natural.

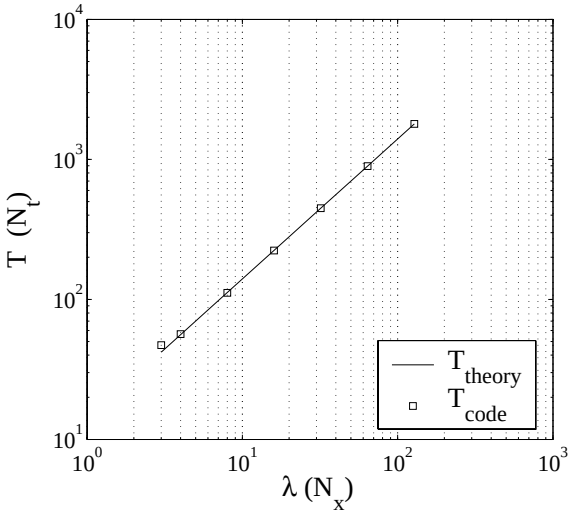

Figure 5.2 Alfven dispersion (real part) for $\mathbf{k} \parallel \mathbf{B}_0$. $\mathbf{k}$ and $\mathbf{B}_0$ that are aligned with the grid, and $\|\mathbf{B}_0\| = 0.1$ giving $\beta \approx 30$.

ν is encouraging: the interface does not appear to be introducing any instability into the scheme. These plots are only motivational. A more convincing test would be to show that the dual-block solution is converging to the single-block solution. We will do this later for a different type of Alfven wave.

We also test the imaginary part of the Alfven dispersion on the single-block. The dispersion relation for an Alfven wave propagating parallel to the background magnetic field with wave-number magnitude k is

$$(\omega - i\eta k^2)(\omega - i\nu k^2) = c_a^2 k^2 \tag{5.28}$$

which reduces to

$$\omega = c_a k + i\eta k^2 \tag{5.29}$$

when $\nu = \eta$. Now, recall from the Chapman-Enskog expansion that η and ν are functions of the relaxation parameters τ_g and τ_f, respectively. Thus, we test the code for a range of η by varying the relaxation parameter τ_g (keeping $\eta = \nu$ so that Eq.(5.29) applies). We recover an estimate of the imaginary part of ω by doing a least-squares fit to the

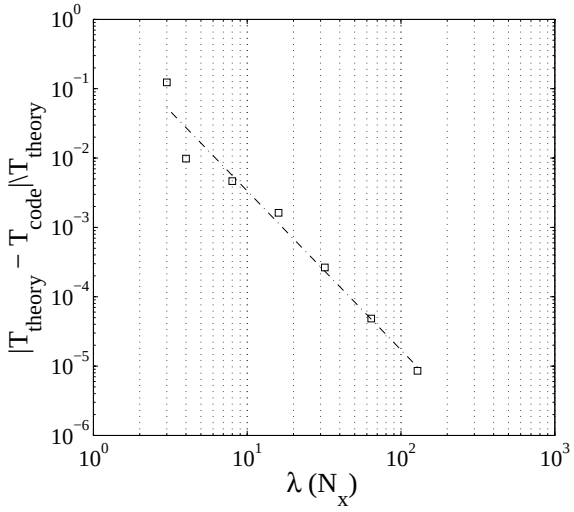

Figure 5.3 Alfven wave dispersion error. The fitted line has slope -2.1.

code output as before. The results are shown in Fig. 5.7. The imaginary part of the dispersion seems to be in good agreement with the predictions from Chapman-Enskog expansion for the tested range of $.001 < \tau_g - 0.5 < .2$.

We next examine the convergence rate of the scheme in δx (or equivalently δt because they are linearly related in the LBM). In this test we propagate an Alfven wave at an a angle of $\frac{\pi}{4}$ with respect to the grid. First, to obtain an effectively exact solution, we propagate the wave for 4 periods on a 256x256 grid. Solutions are then computed on a series of smaller grids: 8x8, 16x16, 32x32, 64x64, and 128x128. We downsample $\mathbf{B}$ in each solution onto an 8x8 grid, and compute the 2-norm of the difference between it and the $\mathbf{B}$ from the 256x256 solution. The results of this procedure are shown in Fig. 5.8. These error values show a convergence rate of -2.08, which is consistent with the second-order rate of convergence we expect.

Fig. 5.9 shows the same result for the dual-block case. In this case, a value of $N_x = 32$ means that the height and width of the entire domain is 32 coarse-sized grid cells (recall that one half of the domain has been refined). The errors are computed with respect to the 256x256 solution on the single-block after appropriate downsampling. In this case

the convergence rate is 1.85. This is again consistent with the expected second-order convergence rate, although slightly less that we might hope. We will discuss a possible explanation for this later. The fact that the dual-block solution is converging to the single-block solution suggests that the multi-block scheme is working successfully.

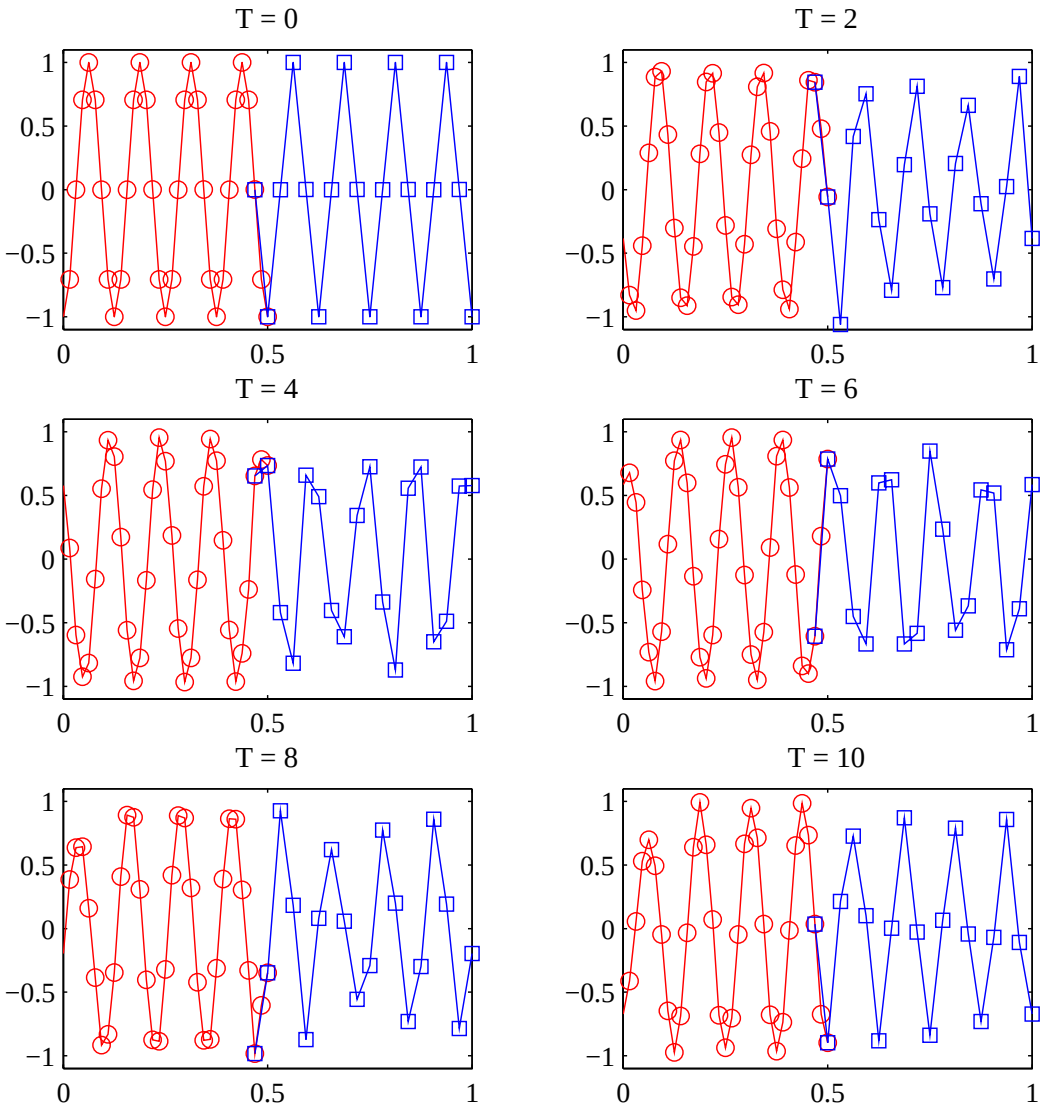

Figure 5.4 $B_z(x, y = 0)/\tilde{B}_z$ at a series of times for an Alfven wave propagation across—and perpendicular to—the boundary between the coarse and fine blocks. Here, $\lambda = 4$ grid points. The period of the oscillation for this wave is 10. For this run, $\eta = \nu = 10^{-6}$.

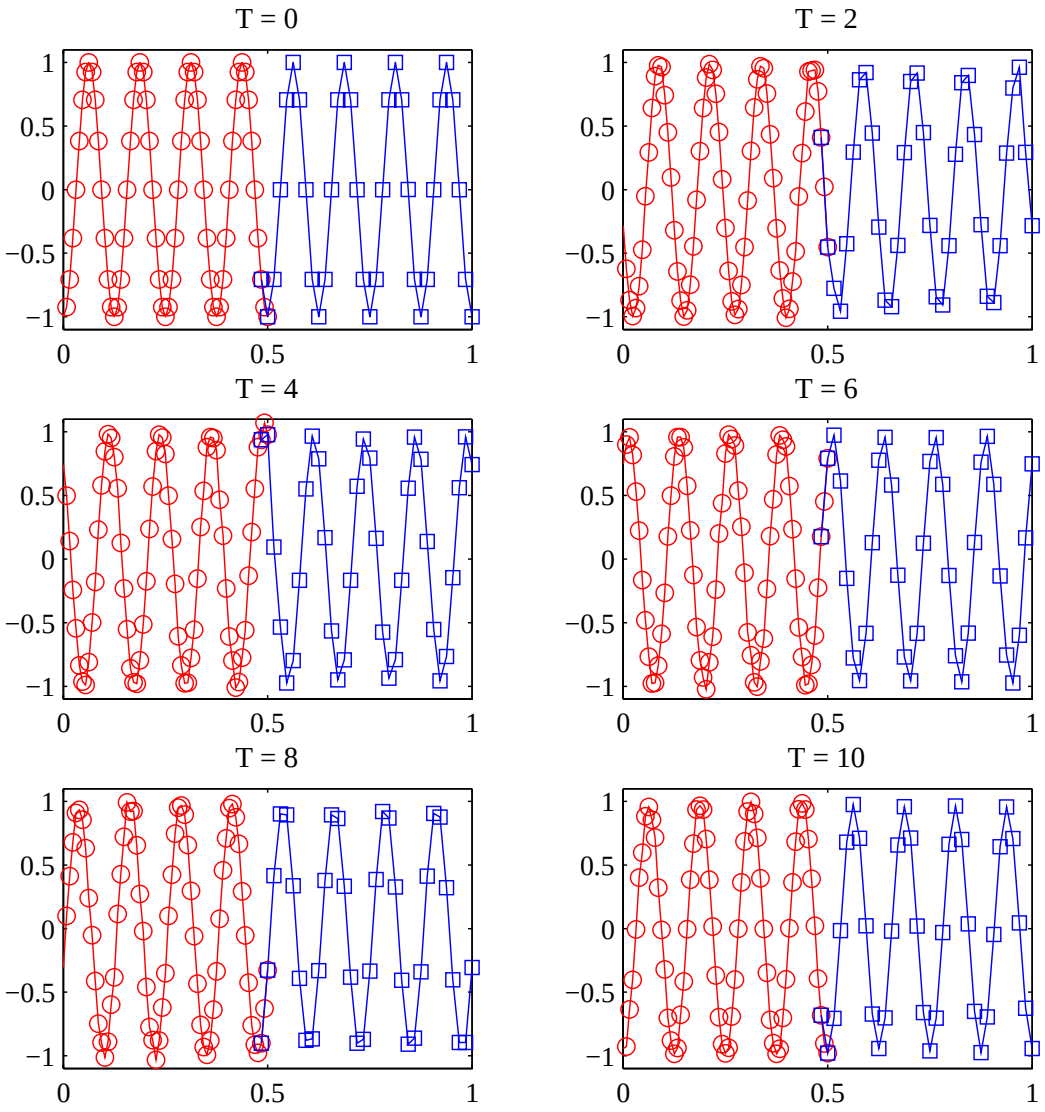

Figure 5.5 $B_z(x, y = 0)/\tilde{B}_z$ at a series of times for an Alfven wave propagation across—and perpendicular to—the boundary between the coarse and fine blocks. Here, $\lambda = 8$ grid points. The period of the oscillation for this wave is 10. For this run, $\eta = \nu = 10^{-6}$.

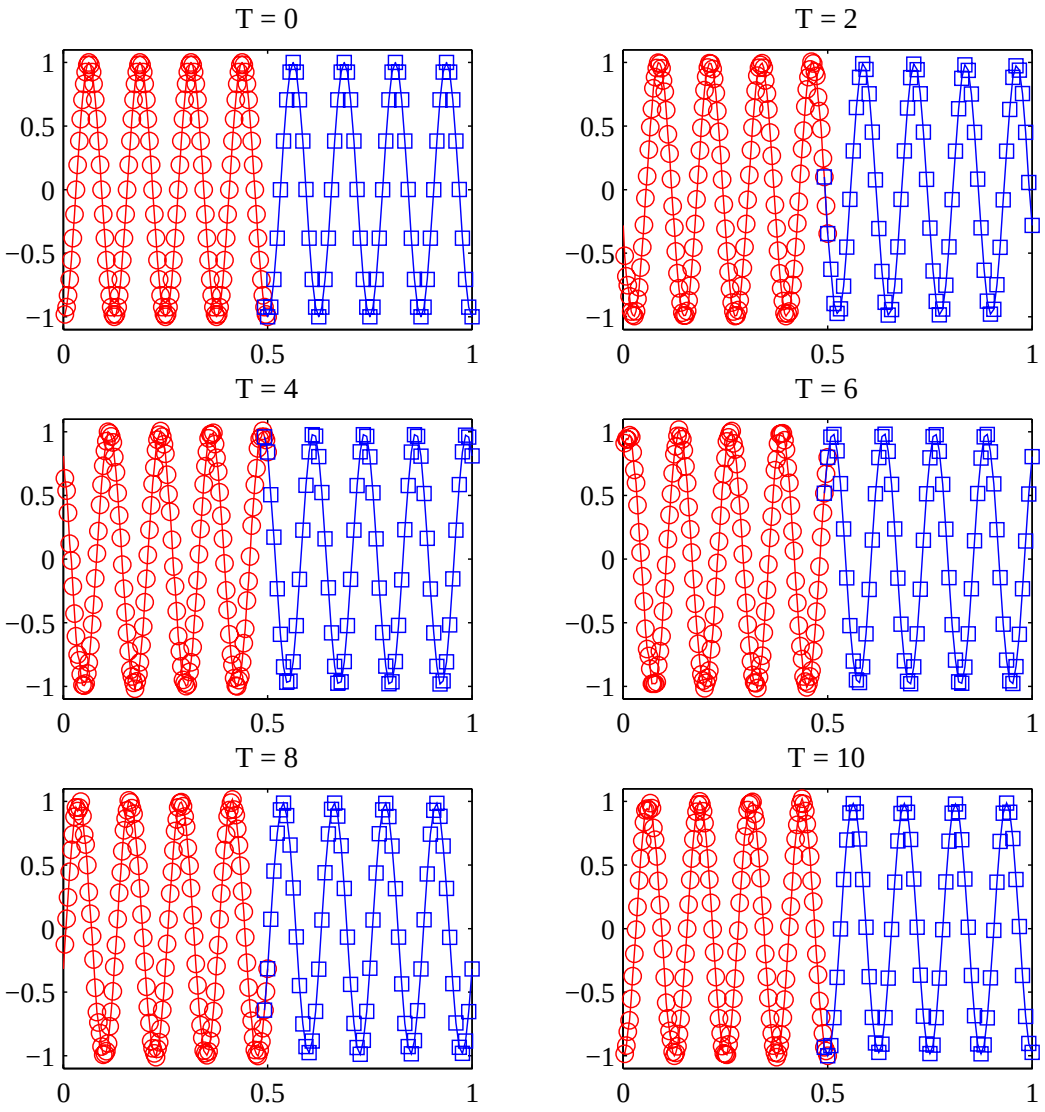

Figure 5.6 $B_z(x, y = 0)/\tilde{B}_z$ at a series of times for an Alfven wave propagation across—and perpendicular to—the boundary between the coarse and fine blocks. Here, $\lambda = 16$ grid points. The period of the oscillation for this wave is 10. For this run, $\eta = \nu = 10^{-6}$.

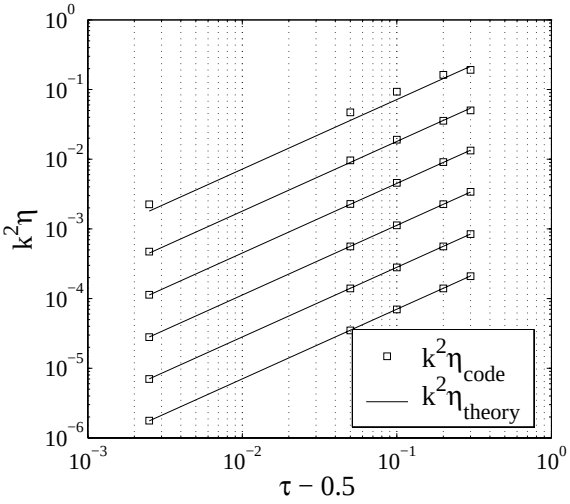

Figure 5.7 Alfven dispersion (imaginary part) for $\mathbf{k} \parallel \mathbf{B}_0$. We use a $\mathbf{k}$ and $\mathbf{B}_0$ that are aligned with the grid, and $\|\mathbf{B}_0\| = 0.1$.

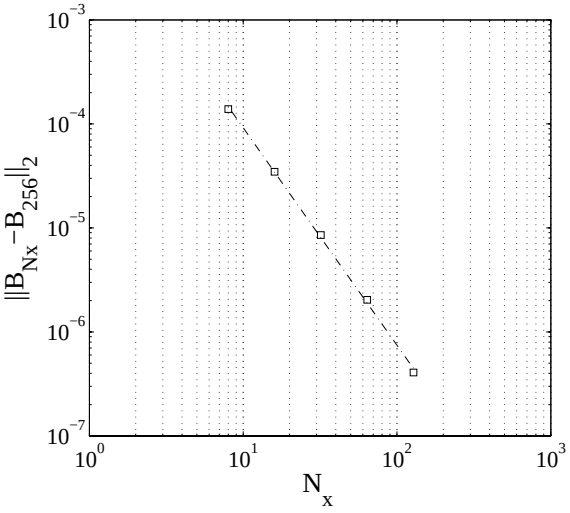

Figure 5.8 Single-block convergence rate for Alfven wave propagating at an a angle of $\frac{\pi}{4}$ with respect to the grid. We have again used $\|\mathbf{B}_0\| = 0.1$. The slope of the fitted line is -2.08, which in consistent with second order convergence in δx.

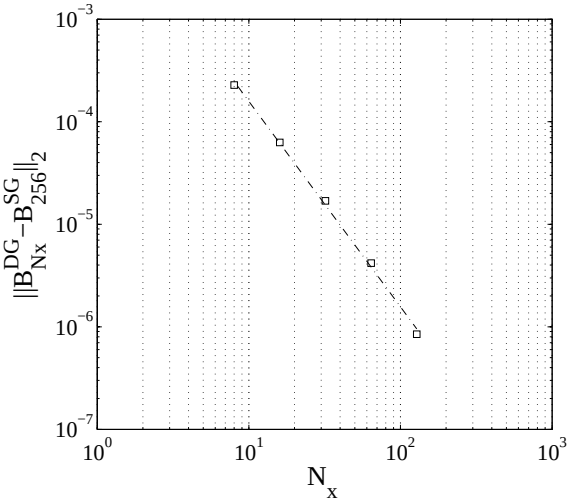

Figure 5.9 Dual-block convergence rate for Alfven wave propagating at an a angle of $\frac{\pi}{4}$ with respect to the grid. We have again used $\|\mathbf{B_0}\| = \mathbf{0.1}$. The slope of the fitted line is -1.85, which in consistent with second order convergence in δx.

5.3 Magnetosonic Dispersion

In this section, we test for the proper reproduction of magnetosonic waves. As before, we setup the field perturbations, this time for a traveling magnetosonic wave. We test fast magnetosonic waves with $\mathbf{k} \perp \mathbf{B}_0$ and $\mathbf{k} \parallel \mathbf{B}_0$.

Before proceeding with the test results, we say a few qualitative words about a possible problem with the stability of the fast magnetosonic waves. Recall that linear stability analysis of numerical schemes for hyperbolic systems requires that the CFL condition

$$\beta \frac{\delta x}{\delta t} > c \tag{5.30}$$

be satisfied for stability. Here, c is the speed of the fastest wave supported by the hyperbolic system, and β is some constant that depends on the numerical scheme. In the case of sound waves in the D3Q19 LBM, this constraint means

$$\beta \frac{\delta x}{\delta t} > c_s = \frac{v}{\sqrt{3}} = \frac{1}{\sqrt{3}} \frac{\delta x}{\delta t}, \tag{5.31}$$

where we have used that $c_s = \frac{v}{\sqrt{3}}$ for consistency with the Navier-Stokes equations, and that $v = \frac{\delta x}{\delta t}$ in order for the streaming step to align with the spatial grid.* Now, in the case of the fast magnetosonic waves in the LBM, the CFL stability condition implies that, for the fastest magnetosonic wave (i.e. when $\mathbf{k} \perp \mathbf{B_0}$),

$$\beta \frac{\delta x}{\delta t} > c_{m_f} = \left[c_s^2 + c_a^2\right]^{\frac{1}{2}} = \left[\frac{1}{3}\left(\frac{\delta x}{\delta t}\right)^2 + \frac{B^2}{\rho}\right]^{\frac{1}{2}}. \tag{5.32}$$

Evidently, for a large enough Alfven speed c_a, the CFL condition will be violated. In standard finite difference schemes one can solve this problem merely by decreasing the time step δt to satisfy the CFL condition; however, in this case, because we have required $c_s = \frac{v}{\sqrt{3}}$ and $v = \frac{\delta x}{\delta t}$, decreasing δt will not help satisfy Eq.(5.32).

*Recall that v is the length of the streaming vector.

Another way of mitigating this problem when the CFL condition is weakly violated is to increase the viscosity and resistivity to dampen any unstable modes. What we found while performing the following tests was that the magnetosonic waves were stable for $\tau_f, \tau_g > 0.5025$ when $\|\mathbf{B}_0\| = 0.1$; however, contrast this with our observation that the Alfven waves were stable for $\tau_f, \tau_g > 0.5 + 10^{-5}$, corresponding to a viscosity and resistivity orders of magnitude lower. We did find that relaxing the requirement $c_s = \frac{v}{\sqrt{3}}$—which has the side-effect of reintroducing more spurious terms into $\mathbf{\Pi}^{(1)}$—can stabilize the magnetosonic wave down to $\tau_f, \tau_g > 0.5 + 10^{-5}$ if we adjust c_s independently of v. Even with this modification, though, the non-linear Orszag-Tang problem still required $\tau_g, \tau_f \approx 0.6$ for stability at moderate Reynolds numbers. This apparent incompatibility between the fast magnetosonic wave stability and the pillars of the LBM derivation (i.e. particles moving with finite, fixed velocity) is something that should be examined in detail if the LBM is to be of wider use for MHD problems.

The results of the fast magnetosonic wave test indicate that fast magnetosonic waves with both $\mathbf{k} \perp \mathbf{B}_0$ and $\mathbf{k} \parallel \mathbf{B}_0$ are being properly reproduced. Fig. 5.10 and Fig.5.11 show the results of extracting the real part of ω using a least-squares fit to the code output. Fig. 5.12 shows the dispersion error for $\mathbf{k} \perp \mathbf{B}_0$. A similar convergence rate was seen for $\mathbf{k} \parallel \mathbf{B}_0$, again showing good convergence as there are more points per wavelength. The only caveat to this result is that, for $\|\mathbf{B}_0\| = 0.1$, we needed to keep $\tau_f, \tau_g > .5025$ for stability, whereas with the Alfven waves we found the scheme stable for a much smaller values of τ_f, τ_g. In any case, for the non-linear Orszag-Tang problem discussed in the next section, we found that we needed $\tau_f, \tau_g > .6$ to maintain stability at moderate Reynolds numbers.

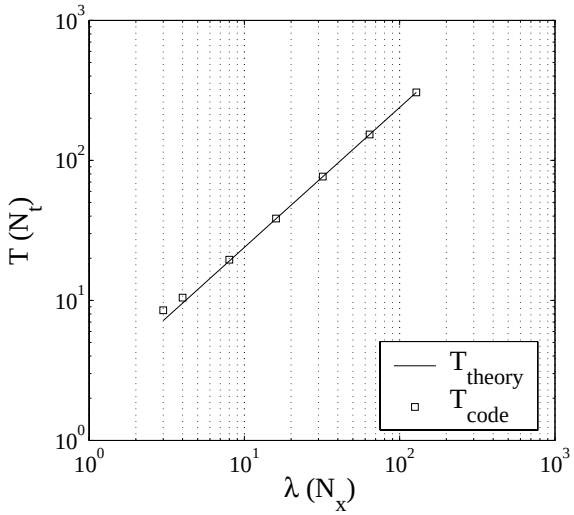

Figure 5.10 Fast magnetosonic dispersion for $\mathbf{k} \perp \mathbf{B}_0$. $\mathbf{k}$ and $\mathbf{B}_0$ are aligned with the grid, and $\|\mathbf{B}_0\| = 0.1$.

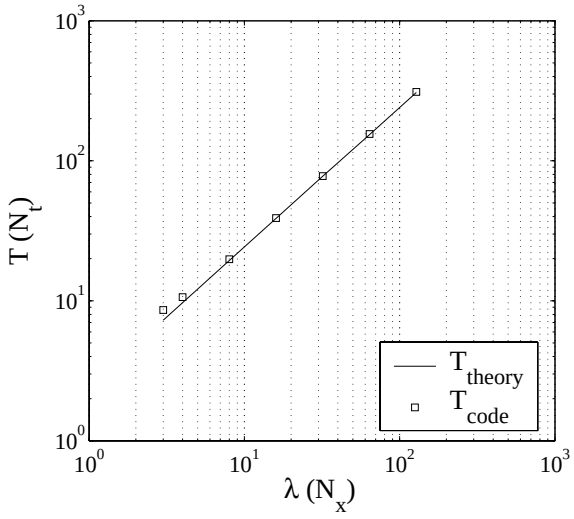

Figure 5.11 Fast magenetosonic dispersion for $\mathbf{k} \parallel \mathbf{B}_0$. $\mathbf{k}$ and $\mathbf{B_0}$ are aligned with the grid, and $\|\mathbf{B}_0\| = 0.1$.

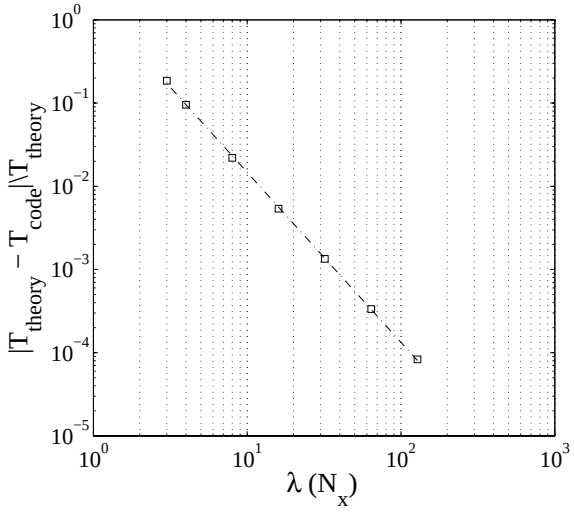

Figure 5.12 Fast magnetosonic dispersion error for $\mathbf{k} \perp \mathbf{B}_0$. The fitted line has slope -2.0.

5.4 Orszag-Tang Problem

We now perform a more stringent, non-linear, test on the code. We examine the behavior of the single-block and dual-block cases for the following initial conditions [18]:

$$\mathbf{B} = \frac{B_0}{2}(\hat{\mathbf{z}} \times \nabla\psi) \quad \text{with} \quad \psi = 2\cos(2\pi x) - \cos(4\pi y) \tag{5.33}$$

$$\mathbf{u} = \frac{u_0}{2}(\hat{\mathbf{z}} \times \nabla\phi) \quad \text{with} \quad \phi = 2(\cos(2\pi x) - \sin(2\pi y)) \tag{5.34}$$

over the domain $0 < x, y < 1$. We choose these initial conditions, due to Orszag and Tang, because they give rise to many of the features of turbulent plasma flow. They are a popular choice for code validation exercises [18]. In [9], the author shows that solutions from a lattice kinetic scheme similar to one derived here converge to solutions computed using a spectral code. The primary purpose for this exercise is to show that the dual-block algorithm converges to the solution computed on the single-block. For what follows, we use $B_0 = 0.2$, and $u_0 = 0.2$, with $\eta = \nu = .004$. This results in magnetic and flow Reynolds numbers of about 50. The Mach number based on peak flow speed is about $\frac{1}{3}$, and $\beta \approx 10$. *

Figures 5.13, 5.14, and 5.15 show the evolution of B_y on 16x16, 32x32, and 64x64 single-block grids. The solution is clearly converging. If we downsample these B_y solutions at $T = 2$ onto an 8x8 grid and compute the difference between this and the 256x256 solution, we get the plot given in Fig. 5.20. These errors show a convergence rate of 2.1, which is consistent with the second order rate of convergence we expect.

Figures 5.16, 5.17, and 5.18 show the evolution of B_y on 16x16, 32x32, and 64x64 dual-block grids. Again, we note that the solution is clearly converging as we decrease the grid spacing. We again compute errors with respect to the 256x256 single-block solution, and find a convergence rate of 1.75 as shown in Fig. 5.21. This convergence rate is somewhat less than predicted and requires an explanation.

*We are constrained to such a low Reynolds number here by our need for the scheme to be stable on the 8x8 grid. On the 256x256 grid, we can achieve Reynolds numbers of about 500.

The author believes this loss in global convergence rate might be explained by use of linear spatial interpolation in moving F and $\mathbf{G}$ from the coarse block to the fine block. Recall that when the distribution functions are propagated from the coarse block to the fine block, we must interpolate to recover values on the intermediate fine block nodes. Because we have adopted a linear interpolation, this will limit the rate at which the solution can converge along the interface. This will in turn hurt the global convergence rate. Note as well that the convergence rate of the linear Alfven wave on the dual-block was also somewhat less than 2.0. Further investigation is needed to determine if these lower convergence rates are due to the interpolation schemes; however, with a convergence rate of 1.75 it is fair to say that the multi-block algorithm is still performing well.

As further evidence, we present in Fig.(5.19) a dual-block run where the fine grid has been refined by a factor of 10 with respect to the coarse grid. We use the same paramters as before in this run. The fact that the code is well-behaved even for such a large refinment ratio in the presence of non-linear flows is more evidence that this scheme is working well.

We next examine the extent to which $\nabla \cdot \mathbf{B} = 0$ is maintained. In Fig. 5.22, we plot the ratio of the max $|\nabla \cdot \mathbf{B}|$ to the max $|\nabla \times \mathbf{B}|$* for the single-block as a measure of how well $\nabla \cdot \mathbf{B} = 0$ is preserved. The plot shows that this ratio decreases as the resolution increases, suggesting that $\nabla \cdot \mathbf{B} = 0$ is being preserved up to truncation error. In Fig. 5.23, we show the same plot for the dual-grid case. This plot shows the same qualitative behavior, suggesting that in the dual-grid we are also preserving $\nabla \cdot \mathbf{B} = 0$ up to truncation error. In each case we compute the the divergence and curl using a second-order finite difference approximation.

Finally, we test that mass is being conserved in the single-block and dual-block cases. In the single-block case, we directly compute the conservation by taking the integral of

*These maxes are taken over the entire domain.

$\rho(t)$ over the domain and subtracting the value of the integral at $t = 0$. Fig. 5.24 shows the results of this procedure for a number of different resolutions. We expect this conservation to be satisfied to near round-off error, which in double precision on an Intel architecture is about 10^{-15}. The figure supports this; however, we note some strange behavior as we vary the size of the grid. Curiously, it appears that a 64x64 grid shows better mass conservation than either an 8x8 grid or a 256x256 grid. We have no *a priori* reason to expect such behavior. In any event, the conservation is clearly satisfactory: while the variations in the density field in this problem are $O(10^{-1})$, the departure from true conservation is at most $O(10^{-14})$, nearly machine round-off.

In the dual-block case we do not expect mass to be absolutely conserved because of the interpolation scheme used to translate F from the coarse to fine grids. What we can show, however, is that the solution for ρ computed on the dual-block is converging to the solution computed on the single-block. This is precisely what Fig. 5.25 demonstrates. The order of convergence here is 1.88. We thus conclude that mass, while not being absolutely conserved as in the dual-block case, is being consistently conserved.

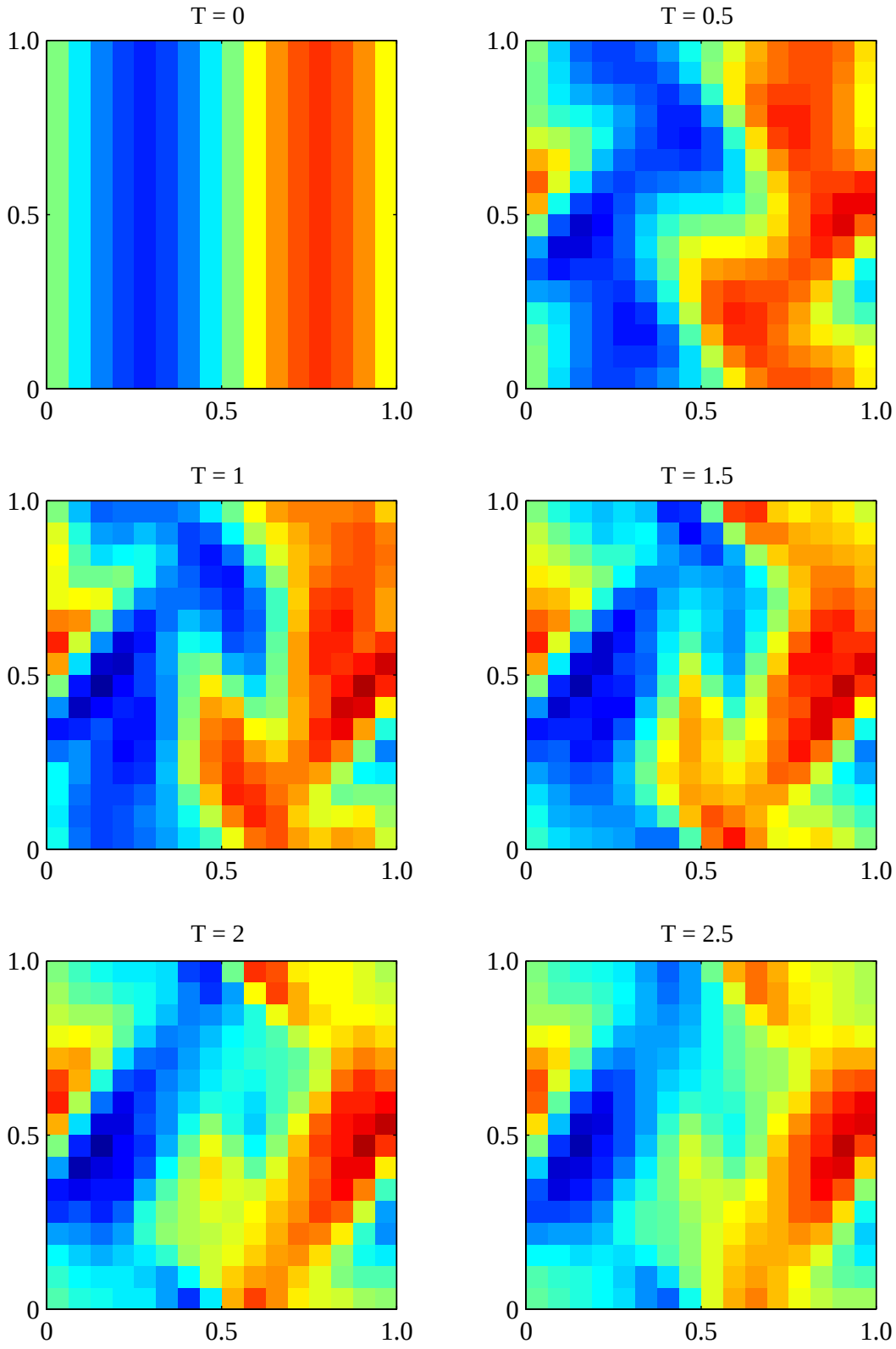

Figure 5.13 Time evolution of B_y for the Orszag-Tang problem on a 16x16 single-block, Re = Rm = 50.

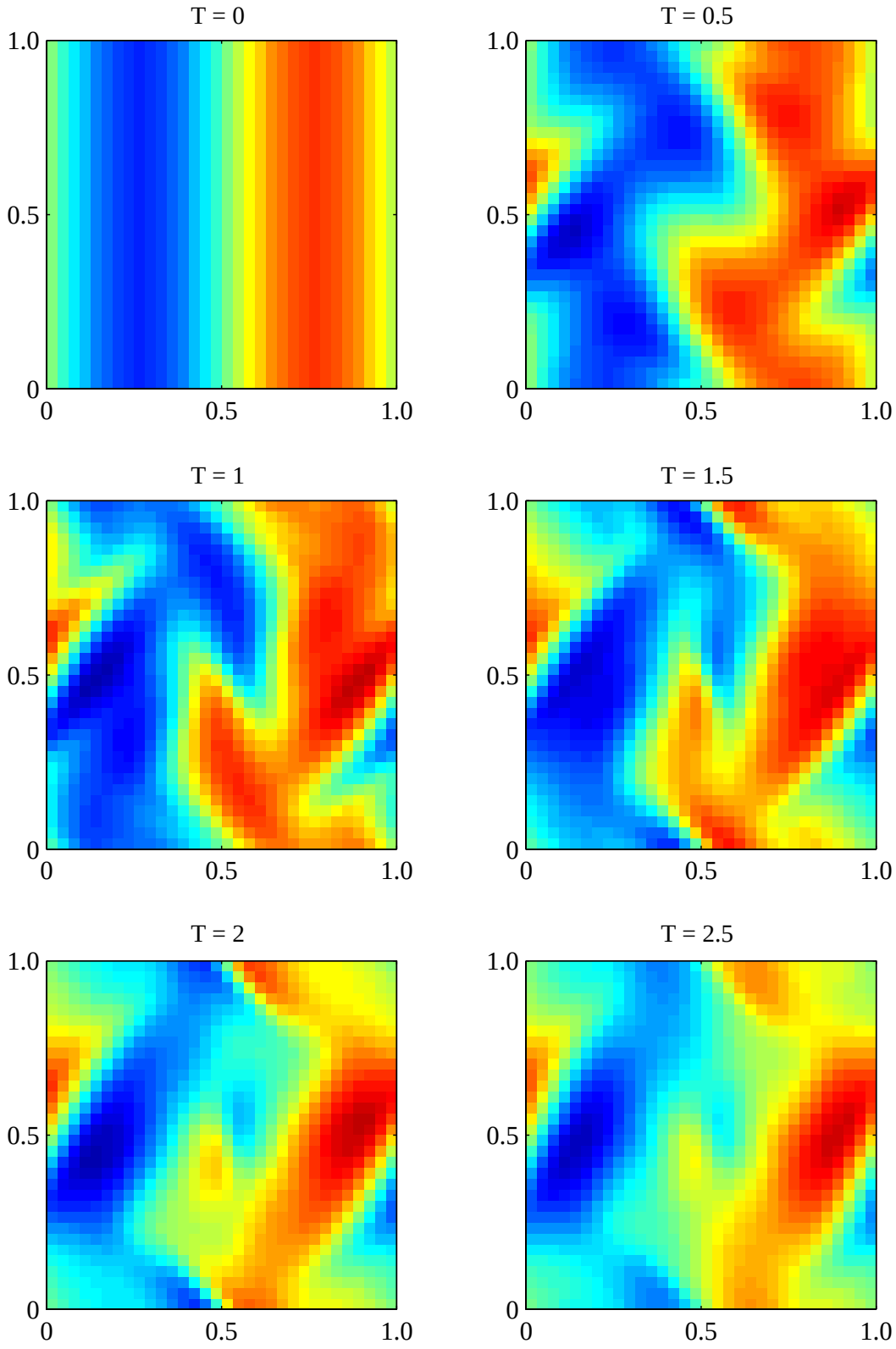

Figure 5.14 Time evolution of B_y for the Orszag-Tang problem on a 32x32 single-block, Re = Rm = 50.

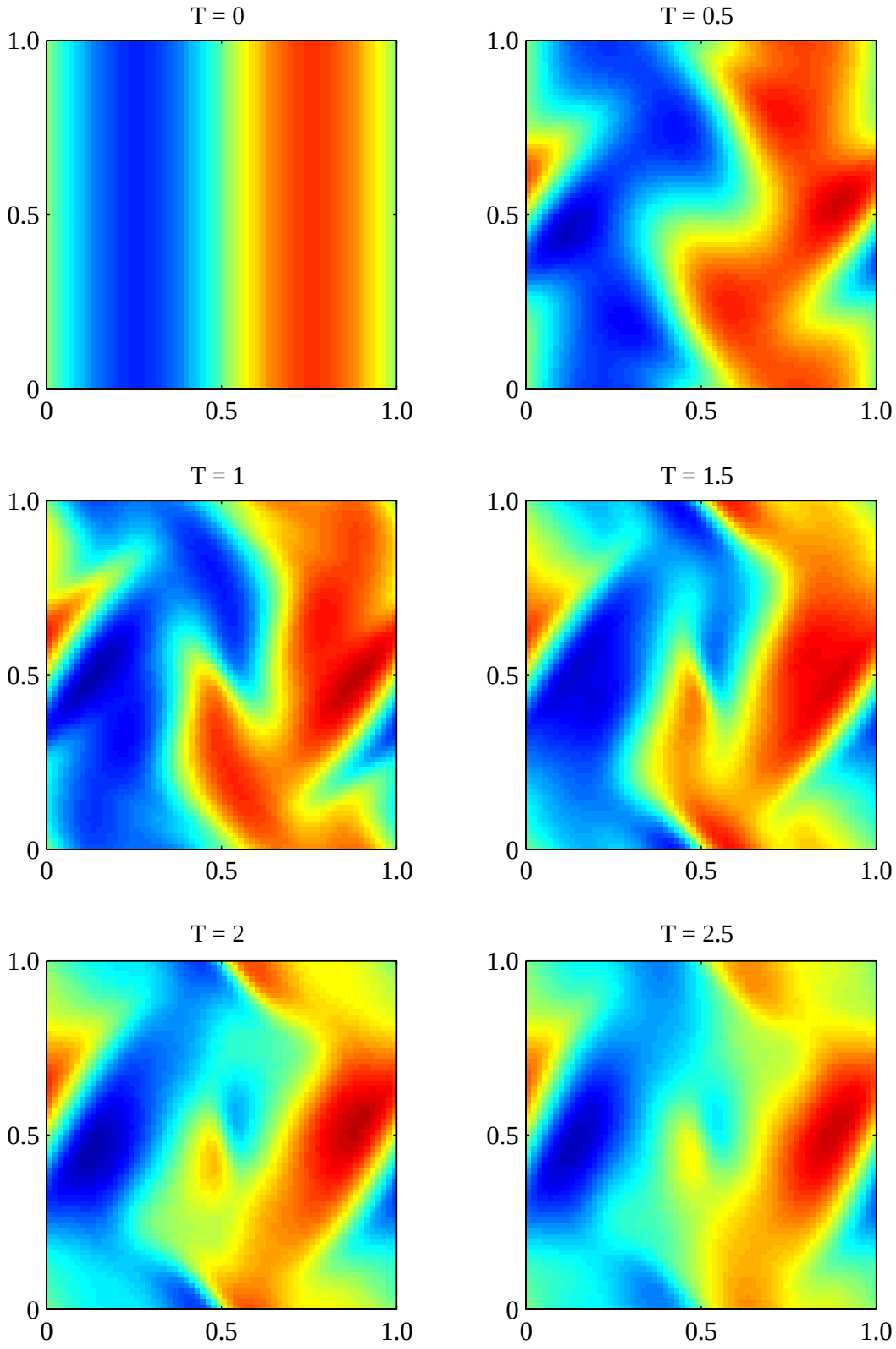

Figure 5.15 Time evolution of B_y for the Orszag-Tang problem on a 64x64 single-block, Re = Rm = 50.

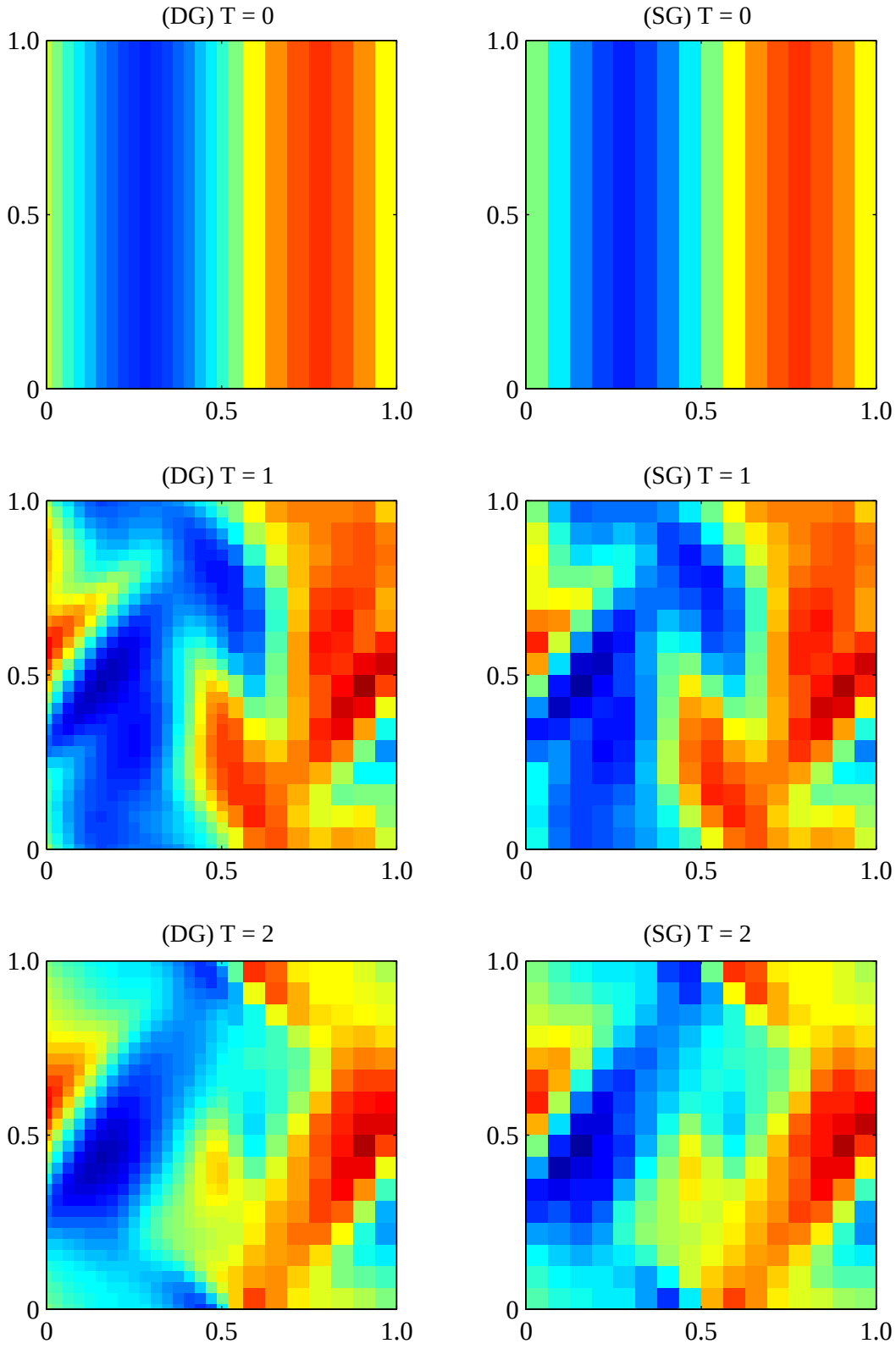

Figure 5.16 Comparison of dual-block(left) and single-block(right) time evolution of B_y for the Orszag-Tang problem on a 16x16 block, Re = Rm = 50.

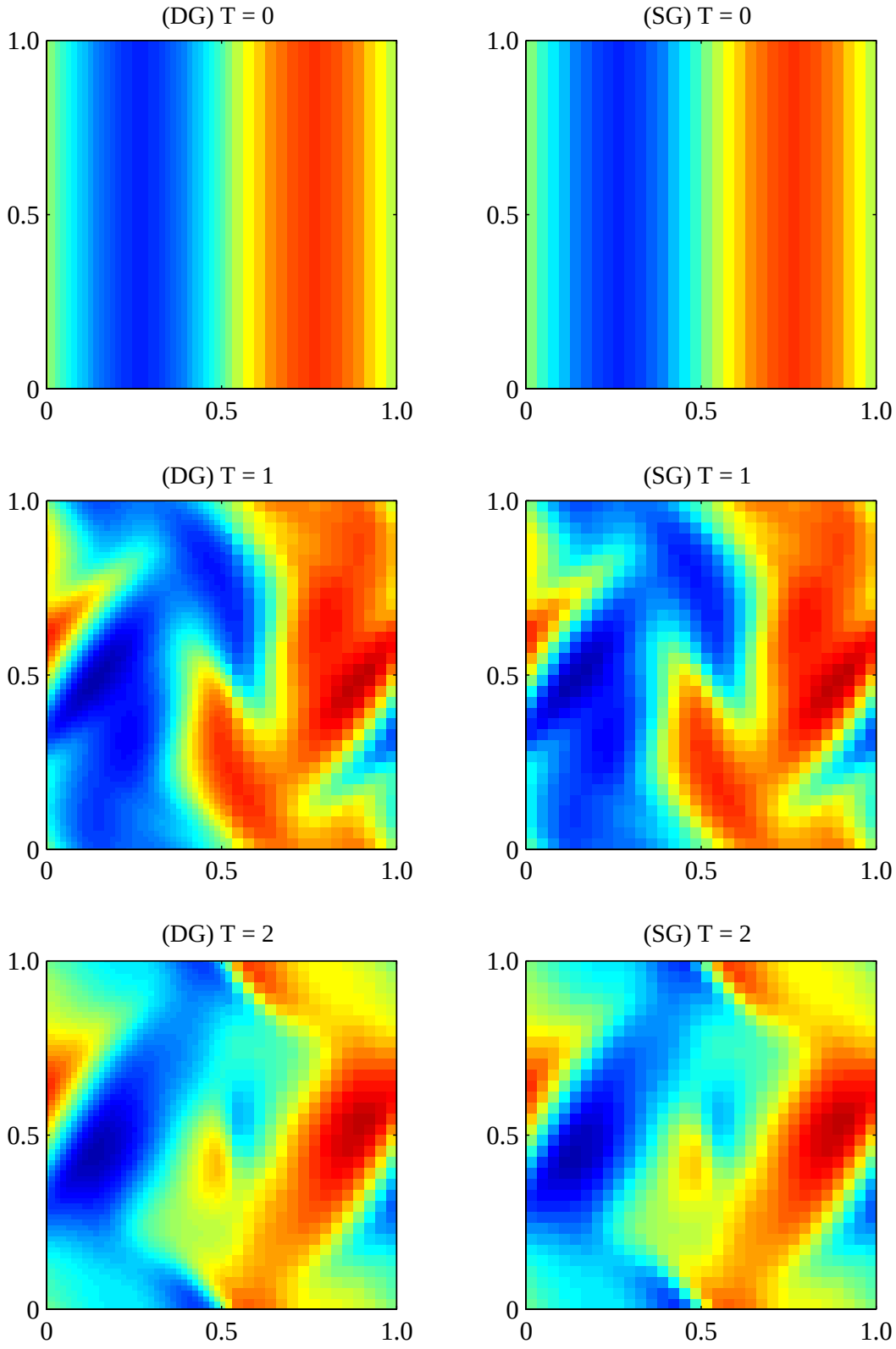

Figure 5.17 Comparison of dual-block(left) and single-block(right) time evolution of B_y for the Orszag-Tang problem on a 32x32 block, Re = Rm = 50.

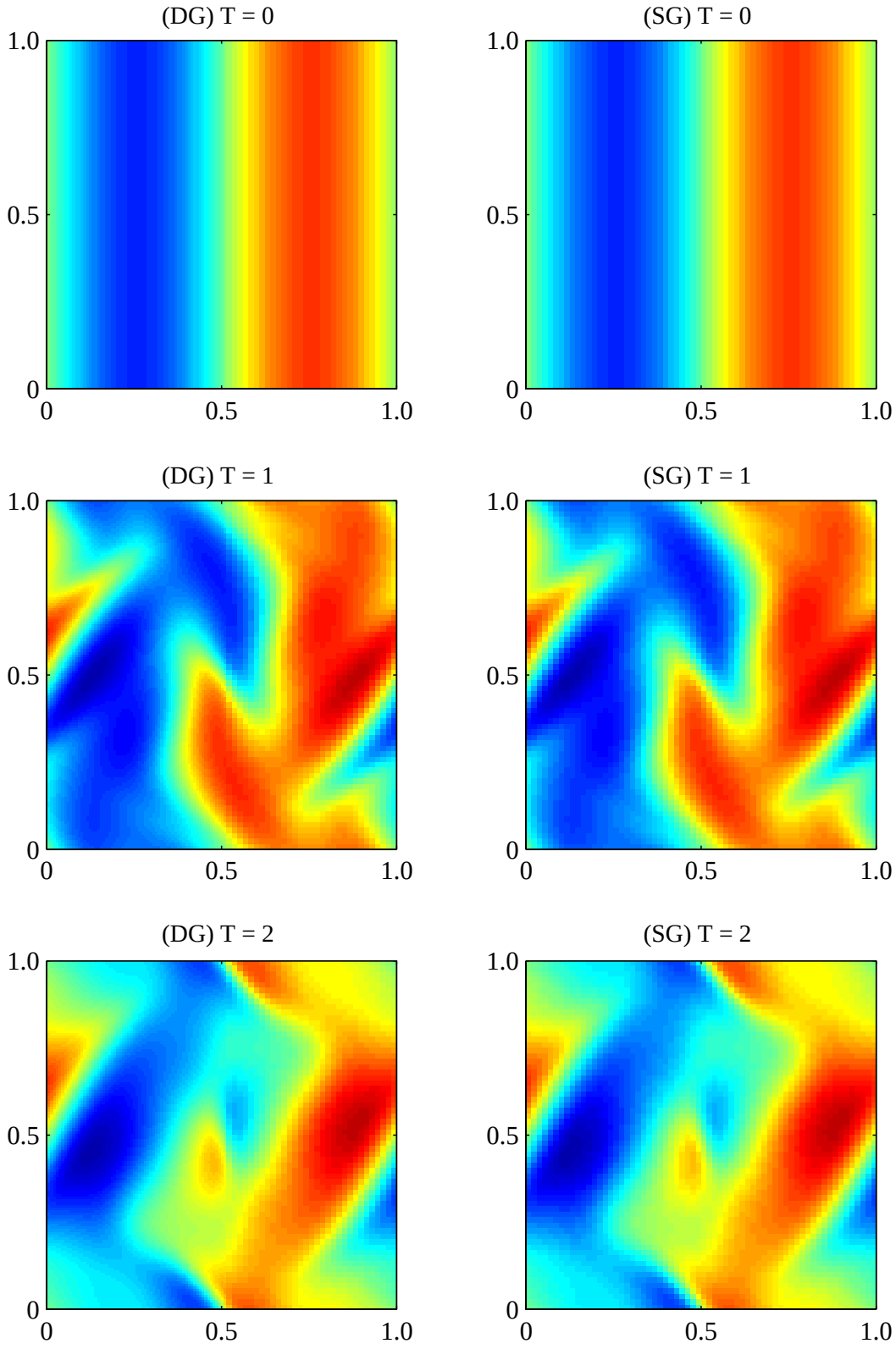

Figure 5.18 Comparison of dual-block(left) and single-block(right) time evolution of B_y for the Orszag-Tang problem on a 64x64 block, Re = Rm = 50.

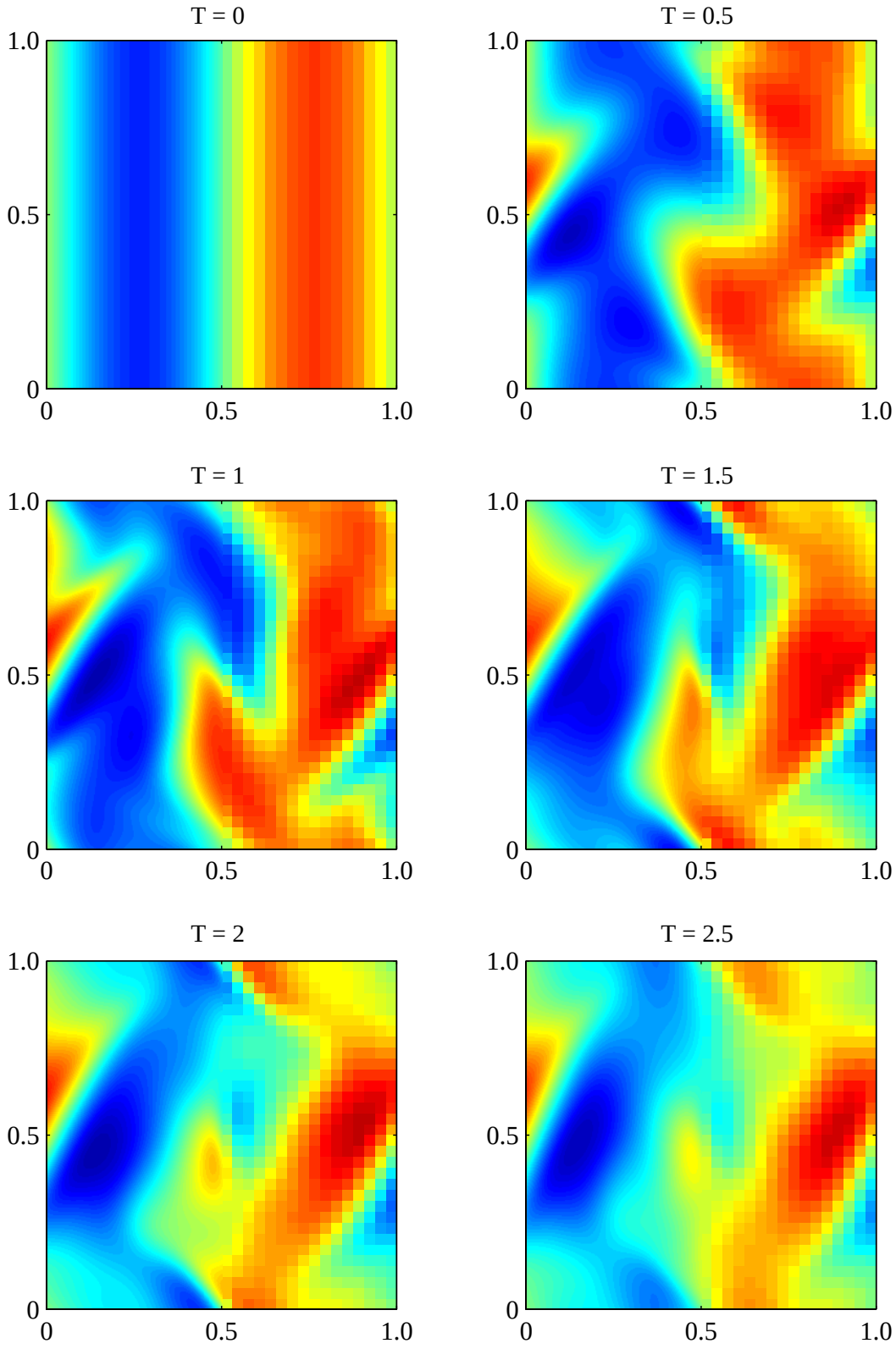

Figure 5.19 Time evolution of B_y for the Orszag-Tang problem on a 32x32 dual-block with 10x refinement on left, Re = Rm = 50.

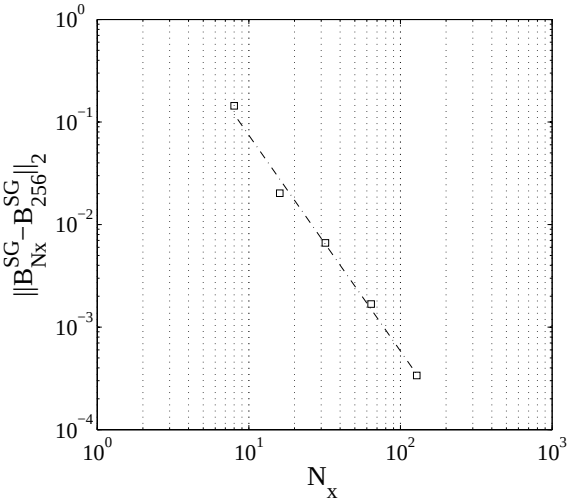

Figure 5.20 Convergence of single-block solution for **B** at $T = 2$ using Orszag-Tang initial conditions for a series of block resolutions. Convergence is computed with respect to the single-block 256x256 solution. Re = Rm = 50. The convergence rate is 2.1.

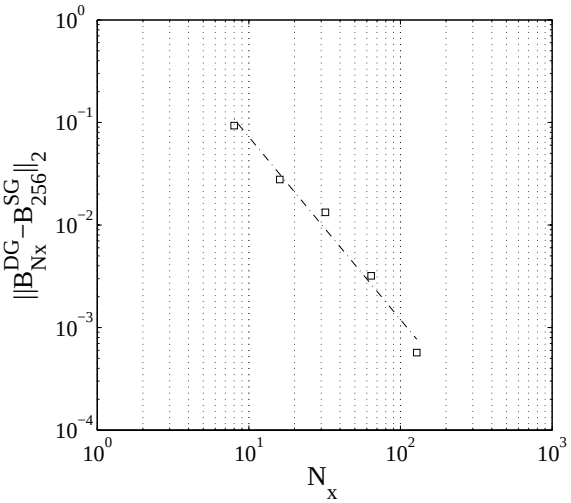

Figure 5.21 Convergence of dual-block solution for **B** at $T = 2$ using Orszag-Tang initial conditions for a series of block resolutions. Convergence is computed with respect to the single-block 256x256 solution. Re = Rm = 50. The convergence rate is 1.75.

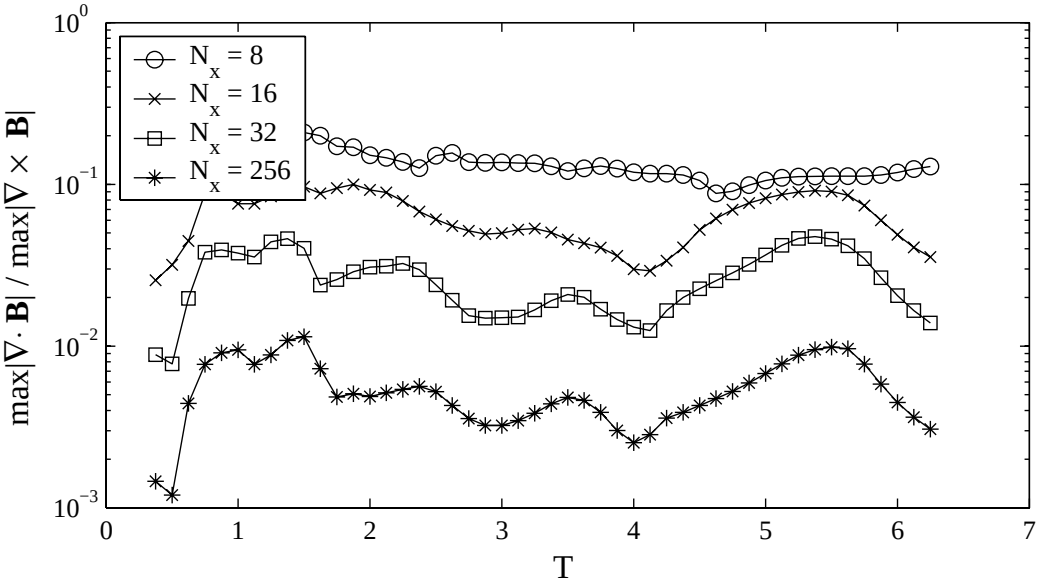

Figure 5.22 $\nabla \cdot \mathbf{B}$ computed for the Orszag-Tang problem on the single-block using a second-order finite difference.

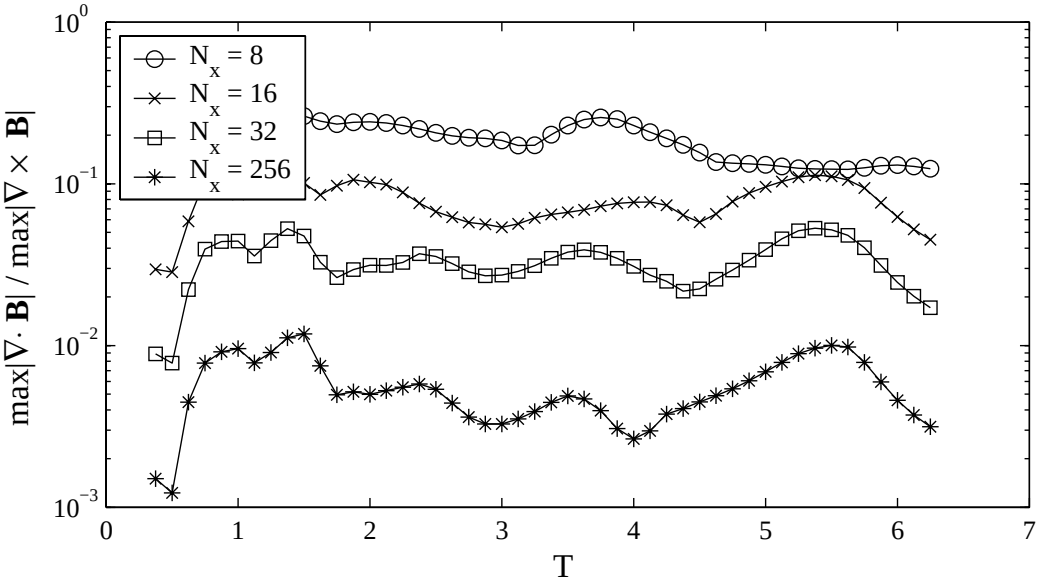

Figure 5.23 $\nabla \cdot \mathbf{B}$ computed for the Orszag-Tang problem on the dual-block using a second-order finite difference.

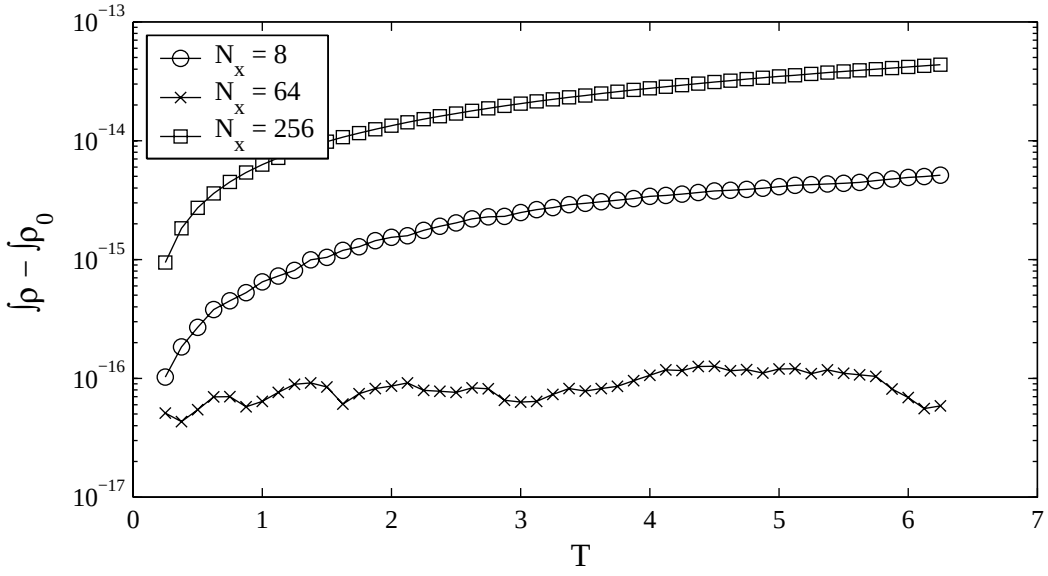

Figure 5.24 Conservation of ρ for the single-block case: $\int(\rho(x,t) - \rho(x,0))dx$.

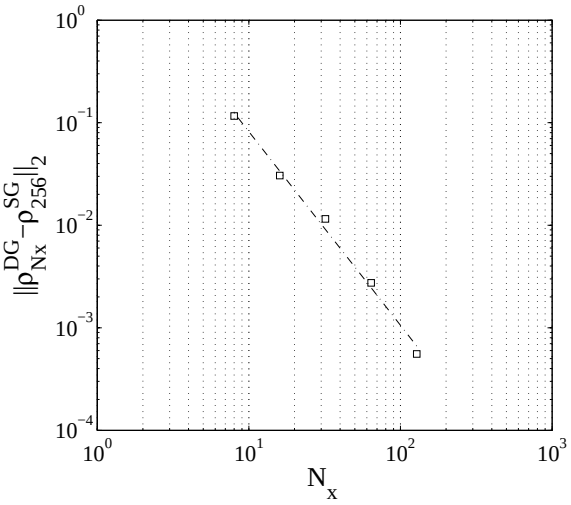

Figure 5.25 Convergence of dual-block solution for ρ at $T = 2$ using Orszag-Tang initial conditions for a series of block resolutions. Convergence is computed with respect to the single-block 256x256 solution. Re = Rm = 50. The convergence rate is 1.88.

Chapter 6
Conclusions

We have developed a lattice kinetic scheme for the 3D resistive MHD equations. The Chapman-Enskog procedure reveals that the scheme is consistent with the MHD equations only in the low-Mach, high-β regime because of spurious terms in $\mathbf{\Pi}^{(1)}$ and $\mathbf{\Lambda}^{(1)}$. The scheme is found to correctly reproduce both the magnetosonic and Alfven waves. The scheme also showed the expected second-order convergence in δx on both the linear Alfven wave and the non-linear Orszag-Tang problem. One issue that remains to be resolved is the method's relatively poor stability at high Reynolds numbers—a problem that is inherent to LBMs in general[9].

Another unwelcome feature of MHD lattice kinetic schemes is the apparent incompatibility of the fast magnetosonic waves and the CFL stability requirement. While it may be possible to fix this problem by adjusting the sound speed independently of the streaming vector length, this approach leads to the re-introduction of extra spurious terms in the viscous part of the stress tensor. In any case, our numerical experiments show that this approach does not help with stability in the non-linear Orszag-Tang problem. More work needs to be done to investigate how to reconcile the fast magnetosonic wave with the CFL stability requirement and to improve the stability of lattice kinetic schemes in general.

One approach to solving these stability issues present in all lattice kinetic schemes is to develop an equilibrium function that satisfies a discrete version of Boltzmann's H theorem. Such methods are unconditionally stable, meaning Reynolds numbers would be limited only by the available resolution. Unfortunately, it has recently been shown that polynomial equilibria—like the one used in this work—cannot satisfy an H theorem [20]; however, some authors have developed entropy methods for the Navier-Stokes equations [2]. These schemes generally require the solution of a non-linear system at each point

in space at each time step to evolve the system. The cost of computing this solution can obviously be prohibitive; however, there is still hope because even these methods preserve the locality that makes the LBM so attractive. Developing a practical entropy scheme for MHD that is unconditionally stable would give the LBM a great advantage over other existing schemes.

Finally, we conclude that the multi-block refinement scheme in [12] can be successfully applied to this lattice kinetic scheme in a pseudo-3D context. All but grid-scale Alfven and magnetosonic waves are shown to propagate well across the boundary interface. The convergence rates obtained with a boundary interface in the domain are slightly lower than the second-order convergence seen without the interface. More investigation is required on this topic to determine the effects of the interpolation schemes on convergence rate. As we discussed before, the linear interpolation scheme used to propagate information from the coarse to fine grids limits the rate of convergence along the interface. Overall though, the multi-block refinement scheme proposed in [12] seems to work well in this context.

Appendix A
Transport Coefficients

In the process of constructing the lattice kinetic scheme for MHD, we found—through successive application of Taylor and multi-scale expansions to the lattice BGK equation—a relationship between the physical transport coefficients η and ν (as they appear in the MHD equations), and the relaxation parameters τ_g and τ_f:

$$\nu = \delta t \left(\tau_f - \frac{1}{2}\right) \frac{v^2}{3} \tag{A.1}$$

$$\eta = \delta t \left(\tau_g - \frac{1}{2}\right) \frac{v^2}{4}. \tag{A.2}$$

The interpretation given in the body of this thesis is that for a certain τ_g and τ_f, we recover the MHD equations with η and ν given above. If one considers that τ_g and τ_f are *free parameters*, it becomes clear that the inverses of Eqs.(A.1) and (A.2)

$$\tau_f = \nu \left(\frac{1}{2} + \frac{3}{v^2 \delta t}\right) \tag{A.3}$$

$$\tau_g = \eta \left(\frac{1}{2} + \frac{4}{v^2 \delta t}\right) \tag{A.4}$$

can be used to *set* τ_g and τ_f to recover a desired η and ν. In this sense, the free parameters τ_g and τ_f can be exchanged for η and ν. It should be emphasized that Eqs.(A.1) and (A.2) are dependent on the equilibirium distribution.

References

1. Bhatnagar P., E. P. Gross and M. K. Krook., A model for the collision processes in gasses. I. Small amplitude processes in charged and neutral one-component systems, *Phys. Rev.* **94**, 1954.

2. Boghosian B., et. al., Galilean-invariant lattice-Boltzmann models with H theorem, *Phys. Rev. E* **68**, 2003.

3. Bouchut, F. Construction of BGK models with a family of kinetic entropies for a given system of conservation laws, *J. Stat. Phys.* **95**, 1999.

4. Chen, H., S. Chen, W. H. Matthaeus., Recovery of the Navier-Stokes equations using a lattice-gas Boltzmann method, *Phys. Rev. A* **45**, 1992.

5. Chen, S., G. D. Doolen., Lattice Boltzmann Method for Fluid Flows, *Annu. Rev. Fluid Mech.* **30**, 1998.

6. Chen, Y., *Lattice BGK Method for Fluid Dynamics: Compressible, Thermal, and Multi-phase Models.* Ph.D. thesis, University of Tokyo, June 1994.

7. Croisille, J.-P., R. Khanfir, and G. Chanteur., Numerical simulation of the MHD equations by a kinetic-type method, *J. Sci. Comput.* **10**, 1995.

8. Dellar, P., Nonhydrodynamic modes and a priori construction of shallow water lattice Boltzmann equations, *Phys. Rev. E* **65**, 2002.

9. Dellar, P., Lattice Kinetic Scheme for Magnetohydrodynamics, *J. Comp. Phys.* **179**, 2002.

10. Dellar, P., Bulk and shear viscosities in lattice Boltzmann equations, *Phys. Rev. E* **64**, 2001.

11. Dupuis, A., B. Chopard., Theory and applications of an alternative lattice Boltzmann grid refinement algorithm, *Phys. Rev. E* **67**, 2003.

12. Filippova, O., D. Hanel., Grid refinement for lattice-BGK models, *J. Comp. Phys.* **147**, 1998.

13. Hou, S. et. al., Simulation of cavity flow by the Lattice Boltzmann Method, *J. Comp. Phys.* **118**, 1995.

14. Jemella, B. D., M. A. Shay, J. F. Drake, B. N. Rogers., Impact of Frustrated Singularities on Magnetic Island Evolution, *Phys. Rev. Lett.* **91**, 2003.

15. Koelman, J.M.V.A., A simple lattice Boltzmann scheme for Navier-Stokes fluid flow, *Europhys. Lett.* **15**, 1991.

16. Macnab, A., *MHD Turbulence: The Development of LBMs for Dissipative Systems.* Ph.D. thesis, The College of William and Mary, 2003.

17. Martinez, D., S. Chen, and W. Mattheaus., Lattice Boltzmann magnetohydrodynamics, *Physics of Plasmas* **1**, 1994.

18. Orszag, S. A., C. M. Tang., Small-scale structure of two-dimensional magnetohydrodynamic turbulence, *J. Fluid Mech.* **90**, 1979.

19. Pavlo, P., G. Vahala, L. Vahala., Higher Order Isotopic Velocity Grids in Lattice Methods, *Phys. Rev. Lett.* **80**, 1998.

20. Yong W., L. Lou., Nonexistence of H-theorems for the athermal lattice Boltzmann models with polynomial equilibria, *Phys. Rev. E* **67**, 2003.

21. Yu, S., R. Mei, W. Shyy., A multi-block lattice Boltzmann method for viscous fluid flows, *Int. J. Numer. Meth. Fluids* **39**, 2002.

22. http://farside.ph.utexas.edu/teaching/plasma/lectures/node64.html.

23. Chen, F. *Introduction to Plasma Physics and Controlled Fusion.* Plenum Press, New York, 1984.

24. Cercignani, C. *The Boltzmann Equation and its Applications.* Springer, New York, 1988.

25. Huang, K. *Statistical Mechanics.* John Wiley and Sons, New York, 1963.

26. Jackson, M. J. *Classical Electrodynamics, 3rd ed.* John Wiley and Sons, New York, 1999.

27. LeVeque, R. J. *Numerical Methods for Conservation Laws.* Birkhauser Verlag, Basel, Switzerland, 1999.

28. Landau, L. D., E. M. Lifshitz. *Fluid Dynamics.* Pergamon, New York, 1959.

29. Wolf-Gladrow, D. *Lattice-Gas Cellular Automata and Lattice Boltzmann Models.* Springer, Berlin, 2000.